Functional characterisation of bicarbonate transporters from the cyanobacterial SbtA2 family and subsequent expression in tobacco

Authors:	**ORCID**	**ResearcherID**
Loraine M. Rourke[1]	0000-0002-2600-8073	OGM-9247-2025
Caitlin S. Byrt[1]	0000-0001-8549-2873	I-9785-2018
Benedict M. Long[1,2,3]	0000-0002-4616-2967	B-3799-2008
G. Dean Price[*,1]	0000-0001-5906-4912	C-9505-2009

[1]Plant Science Division, Research School of Biology, 134 Linnaeus Way, Australian National University, Acton, ACT, Australia, 2601

Current address: [2]Discipline of Biological Sciences, and [3]ARC Centre of Excellence in Synthetic Biology, School of Environmental and Life Sciences, University Drive, The University of Newcastle, Callaghan, NSW, Australia, 2308

[*]To whom correspondence should be addressed: dean.price@anu.edu.au

Running title: SbtA2 transporter function and expression in tobacco

Key words: bicarbonate transporter, chloride dependence, CO_2 concentrating mechanism, cyanobacteria, HCO_3^-, photosynthesis, SbtA2, uptake kinetics.

Highlight

SbtA2 bicarbonate transporters from some marine α-cyanobacteria are high flux transporters with an unusual chloride-dependence and show intermediate uptake affinity when expressed in *E. coli*. Initial attempts failed to demonstrate enhanced photosynthesis when directed to tobacco chloroplasts.

Abstract

Cyanobacteria rely on bicarbonate (HCO_3^-) as the primary inorganic carbon (Ci) source for photosynthesis in aquatic environments. To use of this Ci source, cyanobacteria employ CO_2 concentrating mechanisms (CCMs) that elevate cytoplasmic HCO_3^- via plasma membrane transporters, enhancing carboxylation by carboxysomal Rubisco. The sodium-dependent SbtA1 transporter family is well-characterized in freshwater cyanobacteria, but the related SbtA2 family, prevalent in marine α-cyanobacteria, remains uncharacterised. Here, we report functional characterisation of SbtA2 homologues from marine *Synechococcus* spp., which exhibit high Ci uptake flux with apparent chloride dependence and intermediate HCO_3^- affinity (Km ≈ 150 μM), when assessed in *E. coli*. SbtA2 achieved internal Ci accumulation up to 24 mM within 30 seconds. Co-expression with the putative regulator SbtB2 reduced uptake activity, suggesting a regulatory role for this protein. These findings indicate that SbtA2 transporters contribute significantly to carbon acquisition in marine cyanobacteria. Given potential to enhance CO_2 supply to Rubisco in C_3 plants, we targeted SbtA2 to the tobacco chloroplast inner envelope membrane; however, this did not improve photosynthesis or growth. Our results highlight the functional diversity of cyanobacterial Ci transporters and suggest that additional components may be required for effective transfer of such systems into plant chloroplasts.

Abbreviations

CA	carbonic anhydrase
CAfree	specialized *E. coli* strain that lacks CAs
CCM	CO_2-concentrating mechanism
CO_2	carbon dioxide
Ci	inorganic carbon

C_{int}	intercellular CO_2
HCO_3^-	bicarbonate
IEM	inner envelope membrane
IPTG	isopropyl β-D-1-thiogalactopyranoside
LB	Luria-Bertani
SbtA	sodium-dependent bicarbonate transporter

Introduction

Cyanobacteria are single-celled, photosynthetic organisms of global ecological importance due to their significant contribution to CO_2 fixation into the biosphere (Field *et al.*, 1998; Flombaum *et al.*, 2013). Their acquisition of carbon is primarily driven by the enzyme Rubisco, which fixes CO_2 as part of the Calvin -Benson -Bassham (CBB) cycle for use in cellular metabolism (Badger *et al.*, 2002; Nguyen *et al.*, 2025a). While CO_2 is readily able to permeate cellular membranes, the most abundant form of inorganic carbon (Ci; CO_2, CO_3^{2-}, and HCO_3^-) available for photosynthesis in aquatic environments is the relatively membrane-impermeable bicarbonate ion (HCO_3^-; Falkowski and Raven, 2007). Cyanobacteria and other aquatic photoautotrophs have evolved CCMs to enable the use of this Ci source as a means to elevate CO_2 around Rubisco and maximise carboxylation (Badger *et al.*, 2006; Price *et al.*, 2008). Cyanobacterial CCMs are highly efficient bipartite systems, utilizing Ci transporters to enable active accumulation of HCO_3^- in the cytoplasm, and HCO_3^--permeable micro-compartments called carboxysomes in which Rubisco is encapsulated (Rae *et al.*, 2013a; Nguyen *et al.*, 2025b). Within carboxysomes, a specialized carboxysomal carbonic anhydrase (CA) equilibrates HCO_3^- with CO_2 (Reinhold *et al.*, 1991; Pulsford *et al.*, 2024), thus increasing CO_2 available for carboxylation (Long *et al.*, 2021; Rae *et al.*, 2013b).

There are two main classifications of cyanobacteria based on the form of Rubisco they contain (Badger and Bek, 2008). Using Form-IB Rubisco, β-cyanobacteria are frequently found in smaller freshwater bodies and estuarine habitats, whilst the more abundant α-cyanobacteria (containing Form-IA Rubisco) are widespread in both oceanic and freshwater environments (Badger *et al.*, 2002; Cabello-Yeves *et al.*, 2022). Some α-cyanobacteria are referred to as transition strains

67 and show evidence of genetic inheritance of CCM components by horizontal transfer,
68 often derived from β-cyanobacteria (Rae *et al.*, 2011).
69 The α-cyanobacteria are thought to have a significant impact on global CO_2
70 acquisition into the biosphere due to their relative abundance (Field *et al.*, 1998;
71 Cabello-Yeves *et al.*, 2022) and high rate of CO_2 fixation (Bar-On and Milo, 2019).
72 Estimates suggest as much as 25% of marine primary productivity can be attributed
73 to the predominant α-cyanobacterial genera, marine *Synechococcus* spp. and
74 *Prochlorococcus* spp. (Flombaum *et al.*, 2013).
75 Underpinning CCM function across these phylogenies is a suite of Ci transport
76 systems that support cellular HCO_3^- elevation. Currently, there are five Ci transport
77 systems involved in cyanobacterial CCMs that have been characterised: two CO_2-to-
78 HCO_3^- conversion complexes bound to thylakoid membranes, and three families of
79 plasma membrane HCO_3^- transporters (Price *et al.*, 2008; Long *et al.*, 2016). The
80 HCO_3^- transporters include the constitutively expressed, high affinity/low flux ABC-type
81 transporter BCT1 (Omata *et al.*, 1999; Rottet *et al.*, 2024), the inducible high-
82 affinity/low flux transporter SbtA1 (Shibata *et al.*, 2002; Du *et al.*, 2014), and the low
83 affinity/medium-high flux transporter BicA (Price *et al.*, 2004). Directional conversion
84 of CO_2 -to -HCO_3^- is performed by specialized Type 1 NDH complexes on the thylakoid
85 membranes that use the electron transport chain and specialised CupA/CupB (Walker
86 *et al.*, 2024; Maeda *et al.*, 2002). Both HCO_3^- and CO_2 uptake systems are found in
87 most cyanobacterial species, with the exception of *Prochlorococcus* spp., which
88 generally possess only distant homologues of BicA and SbtA (Rae *et al.*, 2011).
89 Human nutrition relies heavily on C_3 crop plants (Salesse-Smith *et al.*, 2025).
90 However, under current atmospheric conditions, C_3 plants have inefficient
91 photosynthetic processes compared to most other photosynthetic organisms (for
92 instance C_4 plants and phytoplankton) due to a lack of a CCM. CCMs act to increase
93 the concentration of CO_2 at the site of Rubisco, the primary enzyme responsible for
94 carboxylation in photosynthetic organisms (Erb and Zarzycki, 2018). One approach to
95 improve the photosynthetic efficiency of these plants is to transplant a CCM from
96 cyanobacteria into the chloroplast in order to improve CO_2 delivery to Rubisco (Price
97 *et al.*, 2011). However, there is a knowledge gap in the mechanistic and regulatory
98 understanding of cyanobacterial HCO_3^- transporters that needs to be filled before such
99 an ambitious goal can be achieved (Rottet *et al.*, 2021). Modelling indicates that
100 incorporating a carboxysome in the chloroplast stroma, and expression of HCO_3^-

101 transporters in the inner envelope membrane (IEM) of the chloroplast, could increase
102 plant productivity by 36-60% (McGrath and Long, 2014). The expression of a HCO_3^-
103 transporter in the chloroplast IEM alone is also likely to improve photosynthetic
104 efficiency in plants by enhancing net CO_2 supply to Rubisco (Price *et al.*, 2011;
105 McGrath and Long, 2014). HCO_3^- transport proteins have been expressed in the
106 chloroplastic IEM, however there has been little evidence of active HCO_3^- uptake in
107 the chloroplast so far (Rottet *et al.*, 2024; Rottet *et al.*, 2021; Forster *et al.*, 2023; Nölke
108 *et al.*, 2019; Atkinson *et al.*, 2016; Pengelly *et al.*, 2014). While it is unknown as to why
109 this is the case, it is possibly due to a lack of activation mechanisms for foreign
110 transport proteins or incorrect conditions to drive transporter function (Rottet *et al.*,
111 2021). For instance, for Na^+-dependent HCO_3^- transporters such as SbtA1 and BicA,
112 the Na^+ concentration in the cytoplasm (and therefore the cytoplasm:chloroplast
113 stromal Na^+ gradient) may not be optimal for function *in planta*. This demonstrates the
114 need to further understand the function of these HCO_3^- transporters and identify
115 different classes of transporters that could be adapted for use in C_3 chloroplasts.
116 In this study, we focus on the previously undescribed HCO_3^- transporter gene
117 family *sbtA2* (sodium-dependent bicarbonate transporter A2) which is largely found in
118 the α-cyanobacteria (Figure 1; Cabello-Yeves *et al.*, 2022; Rae *et al.*, 2011) and has
119 distant protein homology to the previously characterized sodium-dependent *sbtA1*
120 family (Figure S1; Price *et al.*, 2008; Rae *et al.*, 2011; Du *et al.*, 2014).(Price *et al.*,
121 2008; Rae *et al.*, 2011; Du *et al.*, 2014). Similar to *sbtA1*, the *sbtA2* gene is typically
122 co-located in cyanobacterial genomes with *sbtB2* (Figure S5A-D), coding for a putative
123 regulatory protein SbtB2, homologous to the regulator SbtB1 (Du *et al.*, 2014; Förster
124 *et al.*, 2023; Kaczmarski *et al.*, 2019).
125 Here we characterize the function of several members of the SbtA2 family from
126 α-cyanobacteria in a heterologous bacterial expression system. Genes encoding
127 SbtA2 and SbtB2 from marine α-cyanobacterial species were cloned individually, or in
128 tandem, and expressed in a high-CO_2-requiring (HCR) *E. coli* strain, CAfree (Rottet *et*
129 *al.*, 2024; Forster *et al.*, 2023; Desmarais *et al.*, 2019). SbtA2 homologues that rescued
130 CAfree at ambient CO_2 were further characterized by measuring their HCO_3^- uptake
131 rates, counter-ion dependency and affinity for HCO_3^-. We also assessed the
132 hypothesis that their associated SbtB2 protein acts as a regulator of SbtA2 function in
133 this system. Our results show that like SbtA1:B1, SbtB2 appears to be capable of
134 limiting the activity of its SbtA2 counterpart in *E. coli*. We provide focused analysis of

135 SbtA2 function from *Synechococcus* WH5701 (hereafter SbtA2-WH5701), revealing a
136 potentially different function from its SbtA1 homologue. We then expressed SbtA2 in
137 the chloroplast IEM of *Nicotiana tabacum* to assess its capacity to improve the
138 photosynthetic efficiency of the plants by increasing CO_2 supply to Rubisco.
139
140 **Materials and Methods**
141 Molecular cloning of SbtA2 genes
142 Genes encoding *sbtAB2* from *Synechococcus* WH5701 (accession
143 WP_006170362.1, WP_006170363.1), *Synechococcus* RCC307 (NBQ36408.1,
144 CAK27720.1) and *Synechococcus* CB0205 (WP_010316543.1, WP_010316542.1),
145 *Prochlorococcus* MIT0701 (WP_036914441.1, WP_036914438.1) and
146 *Prochlorococcus marinus* MIT9313 (WP_011130583.1, WP_011130582.1), were
147 synthesized by Genscript (USA) and cloned individually or in tandem under the control
148 of a lac inducible promoter in vectors pCk1 (Kanamycin resistance) or pCsA
149 (Spectinomycin resistance), using type-IIS restriction enzyme cloning that use key
150 features of Golden Gate cloning and Loop Assembly (Pollak *et al.*, 2019; Engler *et al.*,
151 2014). In the absence of a suitable antibody for SbtA2, despite numerous attempts to
152 make one, internal epitope tags were introduced to SbtA2 in the cytoplasmic loop
153 between membrane helices five and six of SbtA2 (Table S3) using the same cloning
154 methods.
155
156 CAfree growth complementation assay
157 A double CA knockout strain of *E. coli* (CAfree; *Δcan ΔcynT*) described by
158 Desmarais et al. (2019), which is unable to grow at air levels of CO_2, was used to
159 screen for HCO_3^- transport. Cultures of CAfree expressing members of SbtA2 were
160 grown in Luria-Bertani (LB) broth at 37°C in air supplemented with 4% CO_2 for 18
161 hours, then diluted 1:5 and grown for an additional hour. The density of the cultures
162 was standardized based on their absorbance (OD_{600} = 0.2) and serially diluted before
163 spotting 10 µL onto LB containing 1.5% agar and appropriate antibiotics (kanamycin
164 – 50 µg/mL or spectinomycin – 100 µg/mL) and 100 µM isopropyl β-D-1-
165 thiogalactopyranoside (IPTG). Plates were incubated overnight at 37°C in air levels
166 (0.04%) and elevated (4%) CO_2 to test for complementation.
167 CAfree growth assay

168 Cultures of CAfree expressing each form of SbtA2 were incubated in LB
169 supplemented with antibiotics (as for the complementation assay) with shaking for 18
170 h at 37 °C in CO_2-supplemented air (4% CO_2). These were diluted 1:5 and grown for
171 approximately 60-90 minutes to achieve log phase growth. Cultures were diluted 1:10
172 into final culture volumes of 200 µL and were grown at 37 °C in 96 well plates in a
173 plate reader (BMG Labtech) under air and CO_2-supplemented-air (4% CO_2) conditions
174 in LB supplemented with antibiotics and IPTG. Growth was measured by taking
175 automated absorbance (OD_{600}) readings at 10-minute intervals for 20 h.

176 Inorganic carbon uptake assay

177 Inorganic carbon uptake was examined in *E. coli* (DH5α strain) expressing
178 *sbtAB2* gene constructs in pCk1 or pCsA (and their derivatives) along with appropriate
179 controls. Starter cultures were grown overnight from a standard glycerol stock in LB,
180 this culture was then diluted 1:5 in LB and grown at 37°C for approximately one hour
181 until absorbance readings (OD_{600}) reached 0.6. Expression was induced by the
182 addition of IPTG to a final concentration of 1 mM, and cultures were grown for an
183 additional 2.5 h at 37°C with shaking. Culture density was measured, and cell volumes
184 adjusted to a standard cell density for each experiment with an approximate OD_{600}
185 1.0-1.2. Cells (~2 mL) were depleted of Ci by washing twice with 1 mL of CO_2-free
186 buffer (20 mM BisTrisPropane-H_2SO_4, pH 7.5, salts as required; sparged with N_2 gas)
187 after centrifugation (20,238 × *g* for 30 s). $NaH^{14}CO_3$ (~60 MBq/mmol) was added to
188 the cells to a final concentration of 0.5 mM and 200 µL of this suspension was
189 overlayed onto 50 µL silicone oil mix AR200:20 3.5:4, above a 20 µL kill solution (3 M
190 sodium hydroxide, 50% methanol) in a 400 µL polypropylene tube (Beckman Coulter).
191 After 30 second incubation the $NaH^{14}CO_3$-cell mix was immediately centrifuged for 20
192 seconds to separate the cells with incorporated ^{14}C from free $NaH^{14}CO_3$ which remains
193 in the supernatant. Tubes were immediately placed in an aluminium block on dry ice,
194 before clipping off the base of the tube containing the cell pellet into scintillation vials
195 containing 400 µL 2 M NaOH. Vials were vortexed well and 2 mL UltimaGold
196 Scintillation cocktail (Perkin Elmer) added before being counted using a Hidex
197 Scintillation counter for 2 minutes. Variations of assay buffer pH, including the
198 concentration of Ci, acid used to pH the buffer, ions added to the uptake buffer and
199 how the $NaH^{14}CO_3$ stock was diluted were also used.

200 To characterise the kinetics of SbtA2 transporters, Ci uptake rates were
201 measured over a range of Ci concentrations to cells expressing each SbtA2. The

202 resulting data were analysed using Michalis-Menten non-linear regression with the
203 statistical fit to assess if the transport kinetics of SbtA2 meets the criteria for active
204 transport.

205 ### Determination of SbtA2 cellular localization in *E. coli*

206 Overnight *E. coli* (DH5α) cultures expressing SbtA2 forms carrying an internal
207 His×6 tag were grown and induced as per Ci uptake assay. Cells were harvested at
208 4,800 × *g* for 5 minutes, washed in lysis buffer (50 mM HEPES-KOH pH 8.0, 100 mM
209 NaCl, 5% glycerol), and left to incubate with ~30 kU of rLysozyme (Merck Millipore)
210 for 30 minutes at 37°C with gentle shaking. Cells were broken using approximately
211 200 µL silica beads using a mini beadbeater-16 homogeniser (BioSpec Products) for
212 5 minutes. Cell debris and beads were removed by centrifugation (20,238 × *g*, 1 minute
213 at room temperature). Supernatants were transferred to clean tubes and membrane
214 enriched fractions collected by centrifugation at 16,700 × *g* in an Eppendorf bench top
215 centrifuge for 30 minutes at 4 °C. Pellets were resuspended in a buffer containing 50
216 mM HEPES pH 8.0, 100 mM NaCl, 25 mM imidazole, and 1% *n*-Dodecyl-*β*-*D*-
217 maltoside (DDM) for 30 minutes on ice to solubilise membrane proteins. Insoluble
218 debris was removed by centrifugation, 16,700 × *g* at 4 °C for 20 minutes, and the
219 supernatant taken was used as the membrane enriched fraction.

220 ### SDS-PAGE and western blot

221 Proteins were separated by SDS PAGE (NuPAGE, 4-12% Bis-Tris mini protein
222 gel, Thermo Fisher Scientific) and subsequently transferred on to PVDF membrane
223 for 45 minutes (BioRad Transblot Turbo). The membrane was blocked with 5% skim
224 milk powder and probed for His×6 or HA tagged proteins using mouse-anti-His×6 or
225 mouse-anti-HA antibodies (and goat-anti-mouse AP-conjugated secondary antibody;
226 Table S5), and developed with Attophos (Promega, USA) prior to imaging on a BioRad
227 Chemidoc MP system as previously detailed (Long *et al.*, 2018).
228

229 ## Plant methods

230 ### Nuclear transformation

231 *Agrobacterium* transformation: *Agrobacterium tumefaciens* (strain GV3101)
232 was transformed with 1µg of pDNA by electroporation, and recovered with 0.5 mL LB
233 at 28°C for 2 h before plating on LB-agar supplemented with 30µg/mL kanamycin and
234 50 µg/mL rifampicin and incubated for ~48 h at 28°C.

235 *N. tabacum* transformation: *Agrobacterium* harbouring plasmid of interest was
236 cultured in LB supplemented with 30 µg/mL kanamycin and 50 µg/mL rifampicin at
237 28°C for 48 h. Cells (~20 mL) were harvested by centrifugation for 10 minutes at 1650
238 × *g*. Cells were suspended in resuspension medium, and left at room temperature for
239 1 h. Sterile tobacco leaves were cut from plantlets growing in tissue culture into 0.4
240 cm^2 pieces and placed adaxial side down on co-cultivation plates with 5 mL of
241 *Agrobacterium* in resuspension medium and left for 5 minutes, before transferring
242 plant pieces to fresh co-cultivation plates. Plates were sealed and left in a controlled
243 temperature growth room at 25°C with 16:8 h photoperiod.
244 After 48 h leaf pieces were transferred to regeneration plates. When shoots
245 appeared, callus with shoots were transferred to fresh regeneration plates and
246 returned to the growth room. When the shoots became big enough to excise they were
247 removed from the leaf pieces and transferred to rooting plates. Once roots had formed,
248 plantlets were transferred to soil (6L of commercial seed raising mix with 2-3 cups of
249 vermiculite and ~25-30 mL of Osmocote) in 8×8 cm^2 punnets in growth chamber.
250 Growth chamber conditions: Temperature was controlled at 25°C daytime/
251 20°C night time, relative humidity 60%, light intensity of 400 µmol s^{-1} m^{-2}, daylength
252 0700-2300 h. After 1-2 weeks, leaf samples (1 cm^2 discs) were taken for determination
253 of the hygromycin resistance gene insert number using droplet digital PCR (iDNA
254 Genetics Ltd, Norwich, UK). Only plants with one insert were continued to the next
255 stages. Leaves were also sampled at this time for immunoblot analysis to assess the
256 expression levels of the transgene. When necessary, plants were transferred to 4.5 L
257 pots filled with steam-sterilised Martins Mix supplemented with 7 g/L Osmocote and
258 moved to the glasshouse to reach maturity prior to seed harvest.
259 For plant growth in glasshouses, pots were placed on benches ~ 1 m off the
260 ground and temperature was controlled to 25°C daytime/20°C night by commercial air-
261 conditioning.

262 ### Plant height, fresh and dry weight determination

263 The height of plants was measured each day from the base of the stem to the
264 base of the apical bud. At 63 days post cotyledon emergence (pce), the above-ground
265 tissue of plants was harvested by cutting at the base of the stem and the entire plant
266 was placed into a paper bag and weighed. The weight of the paper bag was subtracted
267 to determine fresh weight. Plants were then placed in 80°C oven for seven days to dry

268 the plant tissue. The weight of the tissue and bag was recorded, and the weight of the
269 bag subtracted to obtain the dry biomass weight.

270 ### $\Delta^{13}C$ determination of plant biomass

271 Leaf samples (0.5 cm diam discs) were harvested following gas exchange
272 measurements (30 ± 5 cm in height). Samples were placed in 1.5 mL tubes and dried
273 at 80°C for 24 h. The tubes were capped and $\Delta^{13}C$ determination was performed by
274 mass spectrometer at RSB, ANU (Förster *et al.*, 2023)

275 ### Leaf gas exchange measurements

276 Using LI-6800 (LICOR) with a 6 cm^2 aperture, fully expanded leaves of plants
277 with similar size (30 cm ± 5cm) and leaf number were equilibrated to the room for ~20
278 minutes before gas exchange measurements. Leaves were equilibrated at 400 µmol
279 mol^{-1} CO_2 for the reference for 10-20 minutes before starting CO_2 response curves
280 over a series of CO_2 concentrations at two-minute intervals (400, 200, 100, 50,150,
281 250, 400, 600, 800, 1200, 400 µmol mol^{-1} for reference) at a leaf temperature of 25°C,
282 55% relative humidity, and illumination of 1500 µmol s^{-1} m^{-2}.

283 <u>A/C_{int} curves</u> were generated from the data by plotting Assimilation rate (A)
284 against intercellular CO_2 concentration (C_{int}) as calculated in the LI-6800 output.

285 <u>Estimation of CO_2 compensation point</u>

286 The CO_2 compensation point (the intercellular CO_2 concentration where net
287 CO_2 assimilation rate is 0 µmol m^{-2} s^{-1}) was determined from the A/C_{int} curves. The
288 linear part of the curve (0-300 µmol mol^{-1} intercellular C_{int}) was used to determine the
289 compensation point.

290 ### Chloroplast membrane enrichment

291 Chloroplast membrane-enriched protein fractions were isolated from two leaf
292 discs (12 mm^2) that were snap frozen when sampled and stored at -80°C. Samples
293 were ground using Dounce homogenisers with 1 mL of lysis buffer (50 mM EPPS pH
294 8, 5 mM $MgCl_2$, 2 mM DTT, 1 mM Na-diethyl-dithiocarbamate, 0.01g/mL
295 polyvinylpyrrolidone [PVPP]) and 10 µL plant protease inhibitor cocktail (Cat # P9599,
296 Merck Life Science, USA). The suspension was transferred to a 1.5 mL tube, on ice
297 and centrifuged for 30 s at 20,238 × *g* to remove large debris and PVPP. The
298 supernatant was transferred to a new 1.5mL tube and centrifuged for 15 minutes at
299 20,238 × *g* at 4°C. The aqueous supernatant was discarded before resuspending the
300 pellet in wash buffer (50 mM EPPS pH 8, 5 mM $MgCl_2$, 2 mM DTT, 1 mM Na-diethyl-
301 dithiocarbamate, 200 mM NaCl). Centrifugation and washing were repeated twice. All

302 traces of supernatant were removed, and the pellet was resuspended in 50 µL of 2 ×
303 resuspension buffer (4% SDS, 125 mM tris-HCl pH 8.0, 1 mM EDTA pH 8.0) and left
304 at 4°C overnight. The membrane-enriched suspension was centrifuged for 1 minute at
305 20,238 × *g* at 4°C and the soluble fraction was transferred to a new tube.
306 Total protein in the samples was determined using the detergent compatible
307 Bio-Rad DC Protein Assay kit, by diluting the samples 1:10 in 2 × resuspension buffer.
308 Sample (5 µL) or BSA standard was added in triplicate in a 96-well plate, and the kit
309 used as per instruction protocol. Samples were standardised based on total protein
310 values of the samples before being loaded onto SDS PAGE for immunoblot analysis.
311
312 **Results**
313 Based on phylogenetic analysis of multiple protein sequence alignments of
314 SbtA transporter proteins, the well characterised SbtA1 HCO_3^- transporters (Du *et al.*,
315 2014), largely present in freshwater and estuarine β-cyanobacteria, are distinct from
316 homologues found in α-cyanobacteria (Figure 1; Cabello-Yeves *et al.*, 2022; Rae *et*
317 *al.*, 2011; Du *et al.*, 2014). On this basis, we refer here to the former group as SbtA1,
318 and the latter as SbtA2 (Rae *et al.*, 2011). As an example of the phylogenetic distance
319 between SbtA1 and SbtA2 members, sequence identity of SbtA1 and SbtA2 from
320 *Synechococcus* WH5701 is approximately 25% (Figure S1A).
321
322 Heterologous expression and bicarbonate transport function of SbtA2 homologues
323 To evaluate the HCO_3^- transport function of SbtA2 homologues, genes from
324 members of the SbtA2 family (from marine α-cyanobacterial species *Synechococcus*
325 WH5701, RCC307, CB0205, and *Prochlorococcus* MIT0701, and MIT9313) were
326 expressed in the *E. coli* strain CAfree (Desmarais *et al.*, 2019) under the control of the
327 IPTG-inducible *lacI*^{q}*-trc* hybrid promoter (de Lorenzo *et al.*, 1993).
328 The CAfree strain of *E. coli* lacks both CA genes *cynT* and *can* (Desmarais *et*
329 *al.*, 2019) and is therefore incapable of enzymatic HCO_3^--to-CO_2 interconversion within
330 the cytoplasm. This renders CAfree reliant on exogenous CO_2 entry and slow
331 spontaneous chemical conversion to HCO_3^- as a carboxylation substrate to supply
332 anaplerotic pathways in the cell (Merlin *et al.*, 2003). CAfree is unable to grow under
333 atmospheric CO_2 concentrations (~0.04% CO_2) as the rate of HCO_3^- supply is too slow
334 to support these pathways. The subsequent phenotype is a dependency on either
335 high-CO_2 for growth, due to high relative rates of spontaneous HCO_3^- production within

336 the cell, or heterologous expression of either a functional CA (Pulsford *et al.*, 2024) or
337 HCO_3^- transporter (Rottet *et al.*, 2024; Forster *et al.*, 2023) to grow at air levels of CO_2.
338 In our hands we have seen no reversion of this cell line under standard experimental
339 conditions.

340 Of the five SbtA2 family members assessed (chosen as genes with moderate
341 GC content that therefore did not require codon optimisation), three supported growth
342 of CAfree at ambient CO_2 (Figure 2A, S2A). These were from *Synechococcus* spp.
343 WH5701, RCC307 and CB0205; referred to hereafter as SbtA2-WH5701, SbtA2-
344 RCC307 and SbtA2-CB0205 respectively. Neither of the SbtA2 homologues from
345 *Prochlorococcus* spp. (MIT0701 and MIT9313) showed function in CAfree at ambient
346 CO_2 under the complementation conditions assessed (Figure 2A). Functional SbtA2
347 proteins were expressed in *E. coli* strain DH5α and characterised by radiolabelled
348 $NaH^{14}CO_3$ uptake assays using the silicone oil centrifugation-filtration method to
349 determine their HCO_3^- transport activity (Rottet *et al.*, 2024; Du *et al.*, 2014; Forster *et*
350 *al.*, 2023).

351 Previous analysis of members of the SbtA1 family revealed they were
352 Na^{+-}-dependent (Du *et al.*, 2014). Due to their similarity to the SbtA1 family, SbtA2
353 function was initially assessed under similar assay conditions used for SbtA1, namely
354 in the presence of 20 mM NaCl (Du *et al.*, 2014). Under these conditions, we observed
355 high rates of HCO_3^- transport by SbtA2 (Figure 2B, C), particularly for SbtA2-WH5701
356 which had significantly higher flux than SbtA1 from *Synechococcus* PCC7942 (SbtA1-
357 7942) when compared on a cell density basis in the presence of 20 mM NaCl (Figure
358 2B). Typical HCO_3^- uptake rates for SbtA1-7942 were less than 0.5 μmol $Ci{\cdot}OD_{600}^{-1}{\cdot}h^{-1}$
359 (Figure 2B), whereas SbtA2-WH5701 achieved 1-1.5 μmol $Ci{\cdot}OD_{600}^{-1}{\cdot}h^{-1}$ (Figure 2B,
360 C).

361 Since SbtA2 was active in the presence of 20 mM NaCl, we hypothesised that
362 SbtA2 might also be Na^+-dependent. Notably, when SbtA1-7942 was assessed for
363 HCO_3^- uptake in response to Na^+, this Na^+-dependent transporter showed very little
364 uptake in buffers with no added NaCl (Figure 3A). However, SbtA2-WH5701
365 demonstrated elevated rates of HCO_3^- uptake across the range of 0 – 20 mM NaCl
366 (Figure 3A, B), and in the presence of 200 mM NaCl the HCO_3^- uptake rate of SbtA2-
367 WH5701 was as high as 2.5 - 3 μmol $Ci{\cdot}OD_{600}^{-1}{\cdot}h^{-1}$ (Figure 3C).

368 Based on this result, we then assessed which ion, Na^+ or Cl^-, was contributing
369 to the HCO_3^- uptake function by SbtA2, by performing assays in the presence or

370 absence of Na^+ or Cl^- in the uptake assay buffers. SbtA2 HCO_3^- uptake rates were
371 elevated in the presence of NaCl, KCl and LiCl above a control with no added salt, but
372 not in the presence of $NaNO_3$ (Figure 3D), revealing that SbtA2 HCO_3^- uptake activity
373 increased in the presence of Cl^- and not Na^+. This observation was further assessed
374 by measuring the HCO_3^- uptake activity of SbtA2-WH5701 in the presence of NaCl,
375 $MgCl_2$, Na_2SO_4 or $MgSO_4$, revealing the possibility of both Cl^- or SO_4^{2-}-dependency
376 (Figure 3E).
377
378 ## SbtA2 effect on *E. coli* Ci pool sizes
379 Using cell volumes measurements for *E. coli* previously estimated by our group
380 (Du *et al.*, 2014), we calculated the internal Ci pool accumulation for a 30 second
381 period from the addition of 0.5 mM Ci to be 5.5 - 8 mM for SbtA2-WH5701, 2 – 3 mM
382 for SbtA1-7942 and 0.2 mM for the empty vector in the presence of 20 mM NaCl.
383 However, in the presence of 200 mM NaCl, the pool size increased to 15 - 23.5 mM
384 for cells carrying SbtA2-WH5701 and 0.3 mM for cells carrying the empty vector (Table
385 2).
386
387 ## SbtA2 affinity for HCO_3^-
388 HCO_3^- affinity estimates (K_m) were calculated to be approximately 150 - 200 μM
389 for all three SbtA2 homologues from *Synechococcus* in the presence of 20 mM NaCl
390 (Figure 4, S4, Table 1 and Table S4). Maximum HCO_3^- uptake rates for SbtA2-
391 WH5701 in the presence of 100 mM NaCl were approximately double that observed
392 at 20 mM NaCl, but the K_m for HCO_3^- was unaffected by the increased NaCl
393 concentration (Figure 4 and Table 1).
394
395 ## The effect of SbtB2 on SbtA2 HCO_3^- uptake activity
396 Like the *sbtA1* family, *sbtA2* is commonly co-located with *sbtB2* in the genome
397 (Du *et al.*, 2014) (Figure S5). SbtB1 acts to down regulate SbtA1 function when
398 expressed in *E. coli* and cyanobacteria preventing SbtA1 activity (Du *et al.*, 2014;
399 Förster *et al.*, 2023; Fang *et al.*, 2021). We therefore assessed whether the SbtB2
400 protein would affect SbtA2 function in CAfree. Dicistronic constructs of *Synechococcus*
401 SbtA2:B2 with a C-terminal HA-tag on SbtB2 (referred to as SbtA2:B2-HA) were
402 assembled similar to SbtA2 alone, under the control of the *lacI^q-trc* promoter.

403 Complementation of CAfree with SbtA2:B2-HA exhibited similar growth to
404 CAfree expressing SbtA2 alone at ambient CO_2 (Figure 5A, S2B). This suggested that
405 SbtB2-HA does not suppress SbtA2 function in this system. However, $NaH^{14}CO_3$
406 uptake assays using the DH5α strain of *E. coli* co-expressing SbtA2-WH5701 and
407 SbtB2-HA-WH5701 (SbtA2:B2-HA-WH5701) exhibited a ~30% reduction in HCO_3^-
408 uptake activity in comparison to SbtA2 alone (Figure 5B). This suggests SbtB2 has a
409 regulatory role for SbtA2, but not sufficient to completely prevent SbtA2 activity in *E.*
410 *coli*. To determine if the HA tag on SbtB2 was interfering with the likely capacity for
411 SbtB2 to completely inactivate SbtA2, the HCO_3^- uptake activity of SbtA2:B2-WH5701
412 devoid of epitope-tags was also assessed. SbtA2:B2-WH5701 showed similar HCO_3^-
413 uptake activity to SbtA2:B2-HA-WH5701 (Figure 5B). Assessment of alternative
414 expression constructs with protein expression under alternative promoters indicated
415 that the relative abundance of SbtA2 and SbtB2 protein influences the activity of SbtA2
416 (Figure 5C and S5G). Higher expression levels of SbtB2 led to a suppression of SbtA2
417 activity by up to 90% (Figure 5C and S5G).
418
419 Functional characterisation of SbtA2 in *N. tabacum* directed to the chloroplast IEM
420 In order to assess the potential for SbtA2 to improve net CO_2 delivery to
421 Rubisco *in planta*, we expressed SbtA2 in *Nicotiana tabacum* cv Samsun using genetic
422 constructs designed to direct the protein to the chloroplast IEM (Rolland *et al.*, 2016).
423 Two SbtA2 expression constructs with different promoters (*viz*. the tomato Rubisco
424 small subunit promoter; *Sl*RbcS2, and the Arabidopsis ubiquitin promoter; *At*Ub10i)
425 were generated to express an HAH6-tagged form of SbtA2-WH5701 (SbtA2-HAH6-
426 WH5701) in *N. tabacum* cv Samsun.
427 Due to a lack of specific antibody for SbtA2, it was imperative to add an epitope
428 tag to SbtA2-WH5701 in order to detect protein expression. Interestingly, adding a tag
429 at the C- or N-terminus resulted in transporter non-function. However, we
430 demonstrated that SbtA2-WH5701 carrying a tag located in the flexible cytoplasmic
431 loop between transmembrane helices five and six (hereafter the 5-6 loop) had similar
432 HCO_3^- uptake activity as untagged SbtA2-WH5701 (Figure S3, S4). Using this epitope,
433 we were able to determine the relative level of SbtA2-WH5701 expression in
434 transgenic T_2 *N. tabacum* (Tob^{SbtA2}) plants. SbtA2-HAH6 protein expression in Tob^{SbtA2}
435 plants differed across their developmental age, dependent upon the promoter used.
436 SbtA2 protein was more abundant in younger leaves of Tob^{SbtA2} plant lines using the

437 *Sl*RbcS2 promoter, while those lines using the *At*ubi10i promoter had higher SbtA2
438 abundance in older leaves (Figure S6).
439 Tob^{SbtA2} plants appeared similar to wild type (Tob^{WT}) with little to no bleaching
440 of leaves throughout their lifespan (Figure 6H), which has been observed previously
441 in *N. tabacum* expressing SbtA1 proteins (Figure S9). Compared to Tob^{WT}, no
442 differences were observed in relation to photosynthetic performance (CO_2 assimilation
443 rates and derived CO_2 compensation point), final height, or whole plant fresh weight
444 for Tob^{SbtA2} plants (Figure 6). While one *At*ubi10i line ($Tob^{SbtA_ubi\text{-}1.1.3}$) demonstrated
445 an elevated dry weight compared to Tob^{WT} (Figure 6C), and two Tob^{SbtA2} lines had
446 significantly lower $\Delta^{13}C$ values than Tob^{WT} (Figure 6G), these traits were not
447 significantly different across all lines tested.

448 **Discussion**

449 The open-ocean α-cyanobacteria of the *Prochlorococcus* and *Synechococcus*
450 (SynPro) clade is attributed with significant contributions to global CO_2 fixation
451 (Flombaum *et al.*, 2013). Based on the enzyme kinetics of Form-IA Rubisco found in
452 these organisms, cells require the accumulation of at least 10 mM HCO_3^- to approach
453 saturation of CO_2 fixation (>200 μM CO_2) within their α-carboxysomes (Whitehead *et*
454 *al.*, 2014; Shih *et al.*, 2016). In the oceans, available CO_2 levels are less than 15 μM
455 (Young *et al.*, 2016), although HCO_3^- is stably available at around 2 mM (Falkowski
456 and Raven, 2007). This highlights that HCO_3^- uptake has evolved as a feature of
457 biophysical CCMs in many oceanic single-celled algae and cyanobacteria, otherwise
458 conditions would be severely limiting if dependent on diffusive CO_2 uptake alone
459 (Ritchie *et al.*, 1996; Beardall and Raven, 2017). To date, most reports on
460 cyanobacterial HCO_3^- transporters have been on those originating from β-
461 cyanobacteria, and relatively little is known about the Ci uptake systems that power
462 the CCMs of the ecologically important α-cyanobacterial SynPro clade.

463 The type and number HCO_3^- transporters differ in α- and β-cyanobacteria
464 (Cabello-Yeves *et al.*, 2022; Rae *et al.*, 2011). Of the functional cyanobacterial HCO_3^-
465 transporters known (BCT1, SbtA1, BicA), generally the α-cyanobacterial
466 *Synechococcus* clade has genes for one BicA HCO_3^- transporter, while
467 *Prochlorococcus* species have no genes for these HCO_3^- transporters (Cabello-Yeves
468 *et al.*, 2022; Rae *et al.*, 2011). Only distant homologues of SbtA1 and BicA, SbtA2 and
469 BicA2, are apparent in SynPro (Rae *et al.*, 2011). SbtA2 protein sequence identity is
470 only approximately 25% compared to SbtA1 (Figure S1), however, its predicted
471 structure (AlphaFold 3; Abramson *et al.*, 2024) maps with high confidence to that of
472 SbtA1 (Synechocystis PCC6803; PDB: 7egl; Fang *et al.*, 2021 ; Figure S3A-C). This
473 led us to hypothesise that SbtA2 likely functions as a HCO_3^- transporter in species
474 belonging to the SynPro clade.

475

476 SbtA2 functional characteristics

477 In the present study we show for the first time that several members of the
478 SbtA2 family from *Synechococcus* spp. are indeed functional HCO_3^- transporters and
479 displayed an 'always-active' HCO_3^- transport function when expressed in *E. coli*
480 (Figure 2). Compared to SbtA1-7942, SbtA2-WH5701 has a high HCO_3^- transport flux
481 (Figure 2B, 3A, 3C), in fact the highest we have recorded. In the presence of 200 mM

482 NaCl, SbtA2-WH5701 had greater than six times the flux of SbtA1-7942 (Figure 3C).
483 The maximum uptake flux by SbtA2 of 2.5 - 3 μmol·Ci OD_{600}^{-1}·h^{-1} generates an internal
484 Ci pool size of up to 23.5 mM in *E. coli* over a 30 second period, and an accumulation
485 factor of up to 70-fold compared to *E. coli* empty vector controls (Table 2). This extent
486 of accumulation, if translated to a cyanobacterium or a C_3 chloroplast, would be more
487 than enough to reach the levels required to optimally operate the cyanobacterial CCM
488 (Whitehead *et al.*, 2014).
489 Kinetic characterisation revealed that SbtA2 is a medium affinity transporter
490 compared with those previously described (Rottet *et al.*, 2021) exhibiting K_m values of
491 approximately 150 - 200 μM (Table 1). When measured in *E. coli*, SbtA1 from
492 *Cyanobium* PCC7001 and *Picosynechococcus* PCC7002 have affinities for HCO_3^- of
493 189 μM and <100 μM respectively (Du *et al.*, 2014). However, it is likely that more
494 accurate affinities can be measured in model cyanobacteria in future studies since
495 respiratory CO_2 production in heterotrophic *E. coli* can lead to errors in affinity
496 estimates (Du *et al.*, 2014). For instance, the estimates of SbtA1 affinity for HCO_3^-
497 when expressed in cyanobacteria has been measured to be ~2 μM (Price *et al.*, 2004)
498 which is much lower than when measured in *E. coli*. In comparison to the high affinity
499 SbtA1 family, members of the low affinity transporter BicA, have K_m for HCO_3^-
500 estimated to be 75-353 μM when measured in cyanobacteria (BicA from
501 *Synechococcus* WH8102, *Picosynechococcus* PCC7002 and *Synechocystis*
502 PCC6803; Price *et al.*, 2004).
503 Recognizing that the K_m of SbtA2 is well below the Ci concentration present in
504 seawater (Falkowski and Raven, 2007), and the widespread nature of this gene family
505 in α-cyanobacteria, leads us to believe that SbtA2 members could play a critical role
506 in CCMs in this globally important cyanobacterial group. Furthermore, assuming
507 sufficient expression, this indicates that SbtA2 could readily achieve the cytoplasmic
508 HCO_3^- accumulation known to be required in cyanobacteria for efficient CCM activity
509 (Whitehead *et al.*, 2014).
510
511 ## Activation/Energisation of SbtA2 HCO_3^- transport
512 From microbes to animals, HCO_3^- transporters have been shown to function in
513 a multitude of modes, including; HCO_3^-/SO_4^{2-} and HCO_3^-/Cl^- exchangers (some of
514 which are Na^+-dependent; Cordat and Reithmeier, 2014), Na^+/HCO_3^- symporters, K^+-
515 dependent transporters (Parker and Boron, 2013), and ABC-type transporters that rely

516 on ATP for HCO_3^- transport (Omata *et al.*, 1999; Gao *et al.*, 2015). This highlights that,
517 mechanistically, several drivers for HCO_3^- uptake or exchange are entirely feasible
518 and offer potential conceptual frameworks for SbtA2 function.

519 SbtA1 has a distinct requirement for Na^+ for function, typically requiring 10 – 50
520 mM Na^+ for maximum activity when expressed in *E. coli*, and likely a Na^+/HCO_3^-
521 symporter (Shibata *et al.*, 2002; Du *et al.*, 2014). Despite SbtA2 having a predicted
522 structure similar to SbtA1 (Figure S3A-C), evidence here suggests that Na^+ does not
523 drive SbtA2 activity. Instead, both Cl^- or SO_4^{2-} might potentially drive SbtA2 function
524 (Figure 3D, E), noting that Cl^- is substantially more abundant in seawater than SO_4^{2-}
525 (Nessim *et al.*, 2015). SbtA2 demonstrated a high basal rate of HCO_3^- transport when
526 assayed in *E. coli*, which was not improved with additional Na^+ (Figure 3). Moreover,
527 the addition of 100 mM Cl^- or SO_4^{2-} to the assay buffer (in the form of NaCl, KCl, LiCl,
528 $MgCl_2$, $MgSO_4$) resulted in an increase in the HCO_3^- transport flux, approximately
529 doubling the HCO_3^- uptake activity compared to when no additional Cl^- or SO_4^{2-} was
530 added to the uptake buffer (Figure 3).

531 In the heterologous system used here, it is difficult to identify the exact
532 mechanism enabling SbtA2 to transport HCO_3^-. Clearly further work in alterative
533 systems is required to confirm the driving ion flux. Below we propose scenarios as to
534 how Cl^- or SO_4^{2-} may act on SbtA2 function.

535 **HCO_3^-/Cl^- antiport**

536 The results presented in here are consistent with the possibility that SbtA2 may
537 act to exchange HCO_3^- with Cl^- or SO_4^{2-}, moving Cl^- or SO_4^{2-} out of the cell as HCO_3^-
538 is moved in. There are multiple examples of HCO_3^-/Cl^- and HCO_3^-/SO_4^{2-} exchangers
539 (Zhang *et al.*, 2023; Reithmeier, 2001; Reithmeier *et al.*, 2016; Jennings, 2021).
540 Evidence suggests that Cl^- can accumulate in *E. coli* during growth (Schultz *et al.*,
541 1962), likely via H^+/Cl^- exchangers that can actively transport Cl^- (eClC, Garcia-Celma
542 *et al.*, 2013), meaning that cells would have a Cl^- pool capable of driving HCO_3^- uptake
543 via HCO_3^-/Cl^- exchange. This could explain the high basal rate of HCO_3^- transport of
544 SbtA2 in *E. coli*, which is further stimulated with addition of Cl^- (Figure 3), if such an
545 antiport mechanism were in operation. For this mode of action to be observed in *E.*
546 *coli* there would need to be membrane transport systems enabling rapid import of Cl^-
547 to increase HCO_3^- uptake activity by SbtA2. Blocking these Cl^- transporters or
548 measuring their net flux during HCO_3^- uptake may provide evidence that this type of
549 mechanism is in action. For such a mechanism to occur in oceanic cyanobacteria,

550 however, cells would need to hyperaccumulate Cl^- from an external environment that
551 already contains ~500 – 600 mM Cl^- (Nessim *et al.*, 2015) in order to enable gradient-
552 driven HCO_3^-/Cl^- antiport. While Cl^- uptake has been observed (Ritchie, 1992), a
553 mechanism to accumulate and maintain such high internal Cl^- would be required, and
554 seems unlikely (Hagemann, 2011).

555 **HCO_3^-/Cl^- symport**

556 In contrast, it may be possible that SbtA2 acts as a HCO_3^-/Cl^- symporter,
557 transporting Cl^- and HCO_3^- into the cell simultaneously. This seems less likely due to
558 the resulting hyperpolarising effect of the ion influx on the membrane potential of the
559 SbtA2-expressing organism, especially within a marine context. However, this may be
560 possible if there are also active efflux mechanisms involved in the system to regulate
561 cellular Cl^- concentration, preventing hyperpolarization and mitigating the ionic effects
562 of SbtA2 function. Observed rates of HCO_3^- uptake increased when exogenous Cl^-
563 was experimentally elevated in *E. coli* expressing SbtA2 (Figure 3C-E), possibly
564 supporting HCO_3^-/Cl^- symport as a potential mode of action. However, evidence
565 against this mechanism is supported by the elevated base HCO_3^- uptake rate of SbtA2
566 in the absence of SO_4^{2-} or Cl^- (when Hepes buffered solution with pH adjusted to 7.5
567 with KOH was used as the assay buffer; Figure S7). In addition, existing literature does
568 not clearly define HCO_3^-/Cl^- symport as a likely scenario.

569 **Allosteric control by Cl^-/SO_4^{2-}**

570 It is possible that allosteric control by Cl^-/SO_4^{2-} leads to SbtA2 activation.
571 Evidence exists for this mechanism in alternate organisms (Davis-Kaplan *et al.*, 1998;
572 Tulloch *et al.*, 2008; Perutz *et al.*, 1994) and therefore sets a precedence for this type
573 of control. In this scenario, the presence of Cl^-/SO_4^{2-} would alter protein conformation,
574 oligomerisation, or charge around the active site to activate SbtA2, thus enabling
575 transport function. Since SbtA2 exhibits Michaelis-Menten kinetics in Ci response
576 assays (Figure 4 and S4), it is unlikely that SbtA2 is a passive channel and that after
577 allosteric activation by Cl^- a secondary counter-ion (K^+, Na^+, Mg^{2+}) must be required
578 for HCO_3^- transport by SbtA2. If this is the mode of activation for SbtA2, the site of Cl^-
579 $/SO_4^{2-}$ elevation (intracellular or extracellular), the mechanism of Cl^-/SO_4^{2-} action on
580 SbtA2, and the secondary counter-ion would need to be determined to optimise
581 function in non-native environments.

582 These speculative ideas need further investigation to clarify the mode of action
583 of SbtA2, perhaps using $^{36}Cl^-$ to assess Cl^- flux in *E. coli*, or by expressing SbtA2 in

584 *Xenopus* oocytes, or in liposomes where other membrane transport systems may be
585 less likely to confound results. Without further analysis we cannot yet conclude what
586 is the energisation mode for SbtA2. Additionally, expression of SbtA2 in the *Δ5* mutant
587 of *Synechocystis* sp. PCC6803, which has all five Ci uptake mechanisms deleted (Xu
588 *et al.*, 2008), may provide functional information in a cyanobacterial context.
589
590 ***Prochlorococcus* SbtA2**
591 Curiously, the two SbtA2 members from *Prochlorococcus* (Figure 2A) did not
592 function in *E. coli* despite the high sequence similarity of all five homologues (Figure
593 S1). There may be three things to consider here. Firstly, SbtA2's from *Prochlorococcus*
594 may be pseudo-genes, though this seems unlikely since there are so few genes coding
595 for putative HCO_3^- transporters in *Prochlorococcus* genomes (Rae *et al.*, 2011).
596 Secondly, there may be another level of allosteric control that cannot be satisfied in
597 the heterologous *E. coli* expression system. If so, this will require further work to
598 resolve the functional activation of SbtA2 from *Prochlorococcus*. Using an approach
599 such as laboratory evolution to generate functional HCO_3^- transporters has been
600 shown to be useful to resolve important sequence elements contributing to both HCO_3^-
601 transporter and CA function (Pulsford *et al.*, 2024; Rottet *et al.*, 2024). This was
602 attempted on the non-functional members; however, no functional forms have been
603 generated to date in our hands. Thirdly, *Prochlorococcus* species appear to use
604 sulpholipids bilayers (Van Mooy *et al.*, 2006) rather than phospholipid bilayers found
605 in *E. coli*, so there is uncertainty whether *Prochlorococcus* membrane proteins will
606 insert or interact correctly within bacterial membranes. The importance of
607 *Prochlorococcus* as an oceanic contributor to carbon acquisition, and the lack of
608 evidence of any HCO_3^- transport in this genus is intriguing and led us to question how
609 these organisms can be achieving efficient CO_2 fixation in low CO_2 environments
610 without possessing any characterised HCO_3^- transporters. On balance, the most likely
611 scenario is that SbtA2, and/or the distant BicA homologue, are functional HCO_3^-
612 transporters in *Prochlorococcus* spp. or there are alternative HCO_3^- transporters or
613 regulators present that are still undiscovered.
614
615 SbtA2:B2 interaction
616 The SbtB1 protein has been shown to regulate the SbtA1 transporter as a
617 "curfew protein" that inhibits the action of the pump (Förster *et al.*, 2023; Kaczmarski

618 *et al.*, 2019; Fang *et al.*, 2021). Additionally, SbtB1 appears to act as a nucleotide- and
619 redox-sensitive regulator that controls SbtA1 by switching between binding states and
620 promoting AMP-dependent complex formation, possibly modulating HCO_3^- transport
621 in response to cellular energy and light/dark conditions (Selim *et al.*, 2023). In either
622 case, the system is regulated by cellular ATP, or the relative adenylate charge, such
623 that high ATP concentrations lead to the unbinding of the SbtB1 trimer from the SbtA1
624 transport trimer, thereby activating SbtA1 (Förster *et al.*, 2023). Previously, Du *et al.*
625 (2014) showed that SbtA1 activity could be eliminated through co-expression of SbtB1
626 in *E. coli* (DH5α and EDM636 strains). This implies that ATP concentrations inside
627 growing *E. coli* cells must be low enough for SbtB1 to bind SbtA1, resulting in the
628 prevention of SbtA1 function and no growth of *E. coli* (EDCM636 strain) at atmospheric
629 CO_2. Here we found that SbtB2 can inhibit its cognate SbtA2 function by around 30-
630 90% (Figure 5 and S5), depending on protein expression levels, and that the
631 expression level of SbtB2 is important in controlling SbtA2 function. Co-expression of
632 SbtA2:B2 in CAfree did not prevent growth of CAfree *E. coli* at atmospheric CO_2
633 (Figure 5A and S2B). However, HCO_3^- uptake assays in *E. coli* DH5α demonstrated
634 reduced levels of uptake (Figure 5, and S5), and highlights that this is likely sufficient
635 to overcome the CAfree phenotype in growth studies.
636
637 ## The effect of epitope tagging on SbtA2 function
638 Efforts to generate antibodies to SbtA2 for use in immunoblot identification of
639 heterologously expressed protein was unsuccessful. We initially attempted to
640 introduce epitope tags to the N- or C-terminus of SbtA2 but found these resulted in
641 non-functional transporters (Figure S8). Using the predicted structure of SbtA2
642 (Abramson *et al.*, 2024) and the crystal structure of SbtA1 (Fang *et al.*, 2021; Liu *et*
643 *al.*, 2021) as guides (Figure S3), we were able to conclude that the cytoplasmic 5-6
644 loop is a disordered flexible region that may be amenable to epitope tagging.
645 Functional data from tagging studies of SbtA1-7942 suggested this region was not
646 functionally critical in that form of SbtA1 (Du *et al.*, 2014). Here, all assessments of
647 SbtA2 forms carrying an internal epitope-tag within this flexible cytoplasmic 5-6 loop
648 region indicated that these proteins retained function comparable to their untagged
649 counterparts (Figure S3). This understanding was critical to using these SbtA2 forms
650 to assess protein expression in both *E. coli* and tobacco without loss of HCO_3^-
651 transport activity.

652

653 ## Expression of SbtA2 in *N. tabacum*

654 Introduction of CCMs to chloroplasts of C_3 plants has been modelled to boost
655 Rubisco carboxylation, increasing photosynthetic efficiency, thereby improving crop
656 productivity (Price *et al.*, 2011; Rottet *et al.*, 2021; McGrath and Long, 2014) and a
657 possible strategy to circumvent the looming food shortages expected as global
658 population increases (Ray *et al.*, 2013). The expression of functional HCO_3^-
659 transporters in the chloroplast IEM could support a 7-16% increase in crop productivity
660 resulting from increased CO_2 supply to Rubisco (Price *et al.*, 2011; McGrath and Long,
661 2014). Previously several HCO_3^- transporters have been expressed in the chloroplast
662 IEM of model plants, although with mixed results with respect to improvement in
663 photosynthetic parameters. For the most part, there has been no evidence of active
664 chloroplast HCO_3^- accumulation, and where there have been improvements in
665 photosynthetic parameters, this has not been clearly linked to increased CO_2 supply
666 to Rubisco (Rottet *et al.*, 2024; Forster *et al.*, 2023; Nölke *et al.*, 2019; Atkinson *et al.*,
667 2016; Pengelly *et al.*, 2014).

668 Here we successfully directed the epitope-tagged SbtA2-HAH6-WH5701 to the
669 chloroplast IEM of *N. tabacum* after nuclear expression (Figure S6). T_2 plants were
670 assessed for phenotypic and photosynthetic changes to determine the impact of the
671 expressed SbtA2 protein. Although one Tob^{SbtA2} expression line had increased dry
672 matter and two with lower $\Delta^{13}C$ (Figure 6G), there was no consistent improvement of
673 photosynthetic parameters or phenotypic traits of plants expressing SbtA2 compared
674 to wild type (Figure 6). Notably, however, transgenic plant phenotypes appeared
675 similar to wild type plants, and no detrimental effects on plant growth was observed.
676 This contrasts with previous attempts to express SbtA1 in *N. tabacum* which were slow
677 growing and demonstrated a chlorotic phenotype (Figure S9). We conclude from this
678 that SbtA2 may either be non-functional *in planta*, or that the level of function is too
679 low to provide any observable benefit in the lines analysed. It is possible that an
680 alternate SbtA2 homologue may be a better candidate for expression *in planta* (for
681 example SbtA2-CB0205 which appears to have higher activity per unit protein than
682 SbtA2-WH5701 [Figure S3E, F]), or that plant lines showing higher expression across
683 all stages of plant growth might provide a better indication of expected photosynthetic
684 improvements.

685 It still needs to be established with greater certainty if SbtA2 members are in
686 fact Cl^-/HCO_3^- (and/or SO_4^{2-}/HCO_3^-) antiporters, or indeed if they are under $Cl^-/SO4^-$
687 allosteric control. If SbtA2 does rely on Cl^- (or SO_4^{2-}) for HCO_3^- transport function, it is
688 important to understand the existing requirement, magnitude, and maintenance of a
689 Cl^- (or SO_4^{2-}) gradient between the cytoplasm and the chloroplast stroma. This also
690 highlights the pressing need to understand the Cl^- and SO_4^{2-} concentration gradients
691 and movement in leaf tissue sub-compartments and the endogenous transporters
692 involved. This will determine whether the appropriate activation or energisation
693 conditions exist for SbtA2 function in the chloroplast IEM.
694 It is understood that Cl^- is the most abundant anion in the chloroplast
695 (Colmenero-Flores *et al.*, 2019) and serves an important role in photosynthesis as an
696 essential cofactor in photosystem II function (Colmenero-Flores *et al.*, 2019). Cl^-
697 concentrations have been measured at 36-60 mM in chloroplasts of the glaucophyte
698 spinach (Demmig and Gimmler, 1983). Interestingly, similar Cl^- concentrations have
699 been measured in chloroplasts of other important C_3 plants, barley and wheat (39 and
700 48 mM Cl^- respectively; Robinson and Downton, 1984). Additionally, tobacco can
701 accumulate Cl^- in macronutrient quantities without apparent detrimental effects on the
702 plants when grown in elevated Cl^- as long as particular cations are not in excess
703 (Franco-Navarro *et al.*, 2019). Furthermore, growth in elevated NaCl can increase
704 chloroplastic Cl^- concentrations in halophytic plants (Demmig and Winter, 1986). This
705 is an example of a factor that could be optimised in future plant expression studies, if
706 SbtA2 is indeed a Cl^-/HCO_3^- antiporter, or in some way linked to Cl^- availability.
707 However, there are a number of other issues that need optimisation, such as;
708 achieving sustained expression and insertion of SbtA2 targeted to the chloroplast
709 envelope inner membrane, studies to ascertain if a sufficient electrochemical gradient
710 exists between the cytosol and chloroplast stroma, and whether this can be optimised
711 by expression of CLC-type Cl^- importers.
712
713 **Conclusion**
714 This study involved characterisation of a previously undescribed family of
715 HCO_3^- transporters, SbtA2, chiefly found in α-cyanobacteria (Figure 1). Although
716 SbtA2 appears to be a distant relative of the Na^+-dependent SbtA1, the mode of action
717 of SbtA2 is quite different, with an apparent dependency on Cl^- or SO_4^{2-}. SbtA2 also
718 displays high HCO_3^- transport rates, and an affinity for HCO_3^- that can be described

719 as intermediate with respect to other known HCO_3^- transporters. The functional
720 characterisation of SbtA2 in *E. coli* presents as an 'always active' phenotype, which
721 lends itself as a potential candidate for insertion into the IEM of the chloroplast with
722 the aim of improving photosynthetic efficiency in C_3 crop plants. However, *N. tabacum*
723 expressing SbtA2 showed no consistent improvement in photosynthetic parameters
724 compared to wild type plants. Nonetheless, this work highlights that a broader
725 selection of HCO_3^- transporters could have the potential to enhance photosynthetic
726 performance in C_3 plants by delivering Ci to the chloroplast. In order for successful
727 function of SbtA2 *in planta* it is important to understand the apparent Cl^-/SO_4^{2-}
728 dependency of SbtA2 and the concentrations of these ions in sub-compartments in
729 plant leaf tissue, and the consequences of over-expressing SbtA2 and any related ion
730 imbalances this may cause.

731 **Supplementary Data**

732 The following supplementary data are available online.
733 Supplementary Method Epitope tagging of SbtA2.
734 Table S1 Addition of epitope tags to the 5-6 cytoplasmic loop of SbtA2.
735 Table S2 Affinity of H6-tagged SbtA2 homologues for HCO_3^-.
736 Table S3 Antibodies used in this study.
737 Figure S1 Alignment of SbtA homologues across cyanobacteria.
738 Figure S2 Liquid growth assay of CAfree expressing SbtA2±B2.
739 Figure S3 Internal epitope tagging of SbtA2 and functional analysis.
740 Figure S4 HCO_3^- uptake kinetics of tagged and untagged forms of SbtA2.
741 Figure S5 SbtAB2 gene arrangements and SbtB2 co-expression effects on SbtA2
742 HCO_3^- uptake in *E. coli.*
743 Figure S6 Assessment of the localisation and expression of SbtA2 in *N. tabacum*.
744 Figure S7 Analysis of the basal HCO_3^- uptake rate of SbtA2
745 Figure S8 Assessment of N- and C- terminally tagged SbtA2 HCO_3^- transport
746 function and protein expression.
747

748 **Acknowledgements** – The authors thank David Savage (UC Berkeley) for kindly
749 providing the CAfree strain of *E. coli.* We also thank Suyan Yee and Sarah Rottet for
750 carrying out confocal and transient expression analysis, and Kelly Chapman for
751 technical assistance with the Licor6800.
752

753 **Author contributions** – LMR, GDP, BML: conceptualization and visualisation; GDP
754 project administration; LMR: methodology and analysis; BML, GDP, CSB: supervision;
755 LMR: writing – original draft; all authors: writing – review and editing; GDP: funding
756 acquisition.
757

758 **Conflict of interest** - The authors declare no conflicts of interest.
759

760 **Funding Statement** - LMR received an Australian Government Research Training
761 Program Scholarship to cover tuition fees.
762

763 **Data availability** - The primary data supporting this study are publicly available at doi:
764 10.17632/wrwjkyn6bn.1 (Rourke *et al.*, 2025) and are available from the
765 corresponding author upon request. Additional data reported in this paper are
766 presented in the Supplementary Data.

References

Field CB, Behrenfeld MJ, Randerson JT, Falkowski P. 1998. Primary production of the biosphere: integrating terrestrial and oceanic components. Science 281, 237-240.

Flombaum P, Gallegos JL, Gordillo RA, Rincón J, Zabala LL, Jiao N, Karl DM, Li WK, Lomas MW, Veneziano D, Vera CS, Vrugt JA, Martiny AC. 2013. Present and future global distributions of the marine cyanobacteria *Prochlorococcus* and *Synechococcus*. Proceedings of the National Academy of Sciences of the United States of America 110, 9824-9829.

Badger MR, Hanson D, Price GD. 2002. Evolution and diversity of CO_2 concentrating mechanisms in cyanobacteria. Functional Plant Biology 29, 161-173.

Nguyen ND, Rourke LM, Cleaver A, Brock J, Long BM, Price DG. 2025a. Understanding carboxysomes to enhance carbon fixation in crops. Biochemical Society Transactions 53, 671-685.

Falkowski PG, Raven JA. 2007. Aquatic Photosynthesis (Second Edition). Princeton: Princeton University Press.

Badger MR, Price GD, Long BM, Woodger FJ. 2006. The environmental plasticity and ecological genomics of the cyanobacterial CO_2 concentrating mechanism. Journal of Experimental Botany 57, 249-265.

Price GD, Badger MR, Woodger FJ, Long BM. 2008. Advances in understanding the cyanobacterial CO_2-concentrating-mechanism (CCM): functional components, Ci transporters, diversity, genetic regulation and prospects for engineering into plants. Journal of Experimental Botany 59, 1441-1461.

Rae BD, Long BM, Badger MR, Price GD. 2013a. Functions, compositions, and evolution of the two types of carboxysomes: Polyhedral microcompartments that facilitate CO_2 fixation in cyanobacteria and some proteobacteria. Microbiology and Molecular Biology Reviews 77, 357-379.

Nguyen ND, Rourke LM, Price GD, Long BM. 2025b. The Function, Evolution, and Future of Carboxysomes. Journal of Experimental Botany.

Reinhold L, Kosloff R, Kaplan A. 1991. A model for inorganic carbon fluxes and photosynthesis in cyanobacterial carboxysomes. Canadian Journal of Botany 69, 984-988.

Pulsford SB, Outram MA, Förster B, Rhodes T, Williams SJ, Badger MR, Price GD, Jackson CJ, Long BM. 2024. Cyanobacterial α-carboxysome carbonic anhydrase is allosterically regulated by the Rubisco substrate RuBP. Science Advances 10, eadk7283.

Long BM, Forster B, Pulsford SB, Price GD, Badger MR. 2021. Rubisco proton production can drive the elevation of CO_2 within condensates and carboxysomes. Proceedings of the National Academy of Sciences of the United States of America 118, 6118-6118.

Rae BD, Long BM, Whitehead LF, Forster B, Badger MR, Price GD. 2013b. Cyanobacterial carboxysomes: microcompartments that facilitate CO_2 fixation. Journal of Molecular Microbiology and Biotechnology 23, 300-307.

Badger MR, Bek EJ. 2008. Multiple Rubisco forms in proteobacteria: their functional significance in relation to CO_2 acquisition by the CBB cycle. Journal of Experimental Botany 59, 1525-1541.

Cabello-Yeves PJ, Scanlan DJ, Callieri C, Picazo A, Schallenberg L, Huber P, Roda-Garcia JJ, Bartosiewicz M, Belykh OI, Tikhonova IV, Torcello-Requena A, De Prado PM, Millard AD, Camacho A, Rodriguez-Valera F, Puxty RJ. 2022. alpha-cyanobacteria possessing form IA RuBisCO globally dominate aquatic habitats. Isme Journal 16, 2421-2432.

Rae BD, Forster B, Badger MR, Price GD. 2011. The CO_2-concentrating mechanism of *Synechococcus* WH5701 is composed of native and horizontally-acquired components. Photosynthesis Research 109, 59-72.

Bar-On YM, Milo R. 2019. The global mass and average rate of rubisco. Proceedings of the National Academy of Sciences of the United States of America 116, 4738-4743.

Long BM, Rae BD, Rolland V, Forster B, Price GD. 2016. Cyanobacterial CO_2-concentrating mechanism components: function and prospects for plant metabolic engineering. Current Opinion in Plant Biology 31, 1-8.

Omata T, Price GD, Badger MR, Okamura M, Gohta S, Ogawa T. 1999. Identification of an ATP-binding cassette transporter involved in bicarbonate uptake in the cyanobacterium *Synechococcus* sp. strain PCC 7942. Proceedings of the National Academy of Sciences of the United States of America 96, 13571-13576.

Rottet S, Rourke LM, Pabuayon ICM, Phua SY, Yee S, Weerasooriya HN, Wang X, Mehra HS, Nguyen ND, Long BM, Moroney JV, Price GD. 2024. Engineering the cyanobacterial ATP-driven BCT1 bicarbonate transporter for functional targeting to C_3 plant chloroplasts. Journal of Experimental Botany 75, 4926-4943.

Shibata M, Katoh H, Sonoda M, Ohkawa H, Shimoyama M, Fukuzawa H, Kaplan A, Ogawa T. 2002. Genes essential to sodium-dependent bicarbonate transport in cyanobacteria - Function and phylogenetic analysis. Journal of Biological Chemistry 277, 18658-18664.

Du J, Forster B, Rourke L, Howitt SM, Price GD. 2014. Characterisation of cyanobacterial bicarbonate transporters in *E. coli* shows that SbtA homologs are functional in this heterologous expression system. PloS one 9, e115905.

Price GD, Woodger FJ, Badger MR, Howitt SM, Tucker L. 2004. Identification of a SulP-type bicarbonate transporter in marine cyanobacteria. Proceedings of the National Academy of Sciences of the United States of America 101, 18228-18233.

Walker RM, Zhang MQ, Burnap RL. 2024. Elucidating the role of primary and secondary sphere Zn^{2+} ligands in the cyanobacterial CO_2 uptake complex NDH-1_4: The essentiality of arginine in zinc coordination and catalysis. Biochimica Et Biophysica Acta-Bioenergetics 1865, 49149-49149.

Maeda S, Badger MR, Price GD. 2002. Novel gene products associated with NdhD3/D4-containing NDH-1 complexes are involved in photosynthetic CO_2 hydration in the cyanobacterium, *Synechococcus* sp. PCC7942. Molecular Microbiology 43, 425-435.

Salesse-Smith CE, Wang Y, Long SP. 2025. Increasing Rubisco as a simple means to enhance photosynthesis and productivity now without lowering nitrogen use efficiency. New Phytologist 245, 951-965.

Erb TJ, Zarzycki J. 2018. A short history of RubisCO: the rise and fall (?) of Nature's predominant CO_2 fixing enzyme. Current Opinion in Biotechnology 49, 100-107.

Price GD, Badger MR, von Caemmerer S. 2011. The prospect of using cyanobacterial bicarbonate transporters to improve leaf photosynthesis in C_3 crop plants. Plant physiology 155, 20-26.

Rottet S, Forster B, Hee WY, Rourke LM, Price GD, Long BM. 2021. Engineered accumulation of bicarbonate in plant chloroplasts: known knowns and known unknowns. Frontiers in Plant Science 12, 727118.

McGrath JM, Long SP. 2014. Can the cyanobacterial carbon-concentrating mechanism increase photosynthesis in crop species? A theoretical analysis. Plant physiology 164, 2247-2261.

Forster B, Rourke LM, Weerasooriya HN, Pabuayon ICM, Rolland V, Au EK, Bala S, Bajsa-Hirschel J, Kaines S, Kasili RW, LaPlace LM, Machingura MC, Massey B, Rosati VC, Stuart-Williams H, Badger MR, Price GD, Moroney JV. 2023. The *Chlamydomonas reinhardtii* chloroplast envelope protein LCIA transports bicarbonate *in planta*. Journal of Experimental Botany 74, 3651-3666.

Nölke G, Barsoum M, Houdelet M, Arcalís E, Kreuzaler F, Fischer R, Schillberg S. 2019. The integration of algal carbon concentration mechanism components into tobacco chloroplasts increases photosynthetic efficiency and biomass. Biotechnology Journal 14, e1800170.

Atkinson N, Feike D, Mackinder LCM, Meyer MT, Griffiths H, Jonikas MC, Smith AM, McCormick AJ. 2016. Introducing an algal carbon-concentrating mechanism into higher plants: location and incorporation of key components Plant Biotechnology Journal 14, 1302-1315.

Pengelly JJL, Forster B, von Caemmerer S, Badger MR, Price GD, Whitney SM. 2014. Transplastomic integration of a cyanobacterial bicarbonate transporter into tobacco chloroplasts. Journal of Experimental Botany 65, 3071-3080.

Förster B, Mukherjee B, Rourke LM, Kaczmarski JA, Jackson CJ, Price GD. 2023. Adenylnucleotide-mediated binding of the PII-like protein SbtB contributes to controlling activity of the cyanobacterial bicarbonate transporter SbtA. eLife.

Kaczmarski JA, Hong NS, Mukherjee B, Wey LT, Rourke L, Forster B, Peat TS, Price GD, Jackson CJ. 2019. Structural basis for the allosteric regulation of the SbtA bicarbonate transporter by the P(II)-like protein, SbtB, from *Cyanobium* sp. PCC7001. Biochemistry 58, 5030-5039.

Desmarais JJ, Flamholz AI, Blikstad C, Dugan EJ, Laughlin TG, Oltrogge LM, Chen AW, Wetmore K, Diamond S, Wang JY, Savage DF. 2019. DABs are inorganic carbon pumps found throughout prokaryotic phyla. Nature Microbiology 4, 2204-2215.

Pollak B, Cerda A, Delmans M, Alamos S, Moyano T, West A, Gutierrez RA, Patron NJ, Federici F, Haseloff J. 2019. Loop assembly: a simple and open system for recursive fabrication of DNA circuits. New Phytologist 222, 628-640.

Engler C, Youles M, Gruetzner R, Ehnert TM, Werner S, Jones JD, Patron NJ, Marillonnet S. 2014. A golden gate modular cloning toolbox for plants. ACS Synthetic Biology 3, 839-843.

Long BM, Hee WY, Sharwood RE, Rae BD, Kaines S, Lim YL, Nguyen ND, Massey B, Bala S, von Caemmerer S, Badger MR, Price GD. 2018. Carboxysome encapsulation of the CO_2-fixing enzyme Rubisco in tobacco chloroplasts. Nature Communications 9, 3570.

de Lorenzo V, Eltis L, Kessler B, Timmis KN. 1993. Analysis of *Pseudomonas* gene products using $lacI^q$/Ptrp-lac plasmids and transposons that confer conditional phenotypes. Gene 123, 17-24.

Merlin C, Masters M, McAteer S, Coulson A. 2003. Why is carbonic anhydrase essential to *Escherichia coli*? Journal of bacteriology 185, 6415-6424.

Fang S, Huang X, Zhang X, Zhang M, Hao Y, Guo H, Liu LN, Yu F, Zhang P. 2021. Molecular mechanism underlying transport and allosteric inhibition of bicarbonate transporter SbtA. Proceedings of the National Academy of Sciences of the United States of America 118, e2101632118.

Rolland V, Badger MR, Price GD. 2016. Redirecting the cyanobacterial bicarbonate transporters BicA and SbtA to the chloroplast envelope: soluble and membrane cargos need different chloroplast targeting signals in plants. Frontiers in Plant Science 7, 185-185.

Whitehead L, Long BM, Price GD, Badger MR. 2014. Comparing the *in vivo* function of alpha-carboxysomes and beta-carboxysomes in two model cyanobacteria. Plant physiology 165, 398-411.

Shih PM, Occhialini A, Cameron JC, Andralojc PJ, Parry MAJ, Kerfeld CA. 2016. Biochemical characterization of predicted Precambrian RuBisCO. Nature Communications 7, 10382-10382.

Young JN, Heureux AMC, Sharwood RE, Rickaby REM, Morel FMM, Whitney SM. 2016. Large variation in the Rubisco kinetics of diatoms reveals diversity among their carbon-concentrating mechanisms. Journal of Experimental Botany 67, 3445-3456.

Ritchie RJ, Nadolny C, Larkum AWD. 1996. Driving forces for bicarbonate transport in the cyanobacterium *Synechococcus* R2 (PCC 7942). Plant physiology 112, 1573-1584.

Beardall J, Raven JA. 2017. Cyanobacteria vs green algae: which group has the edge? Journal of Experimental Botany 68, 3697-3699.

Abramson J, Adler J, Dunger J, Evans R, Green T, Pritzel A, Ronneberger O, Willmore L, Ballard AJ, Bambrick J, Bodenstein SW, Evans DA, Hung CC, O'Neill M, Reiman D, Tunyasuvunakool K, Wu Z, Zemgulyte A, Arvaniti E, Beattie C, Bertolli O, Bridgland A, Cherepanov A, Congreve M, Cowen-Rivers AI, Cowie A, Figurnov M, Fuchs FB, Gladman H, Jain R, Khan YA, Low CMR, Perlin K, Potapenko A, Savy P, Singh S, Stecula A, Thillaisundaram A, Tong C, Yakneen S, Zhong ED, Zielinski M, Zidek A, Bapst V, Kohli P, Jaderberg M, Hassabis D, Jumper JM. 2024. Accurate structure prediction of biomolecular interactions with AlphaFold 3. Nature 630, 493-500.

Cordat E, Reithmeier RAF, eds. 2014. Structure, function, and trafficking of SLC4 and SLC26 anion transporters. Burlington: Elsevier Inc. Academic Press.

Parker MD, Boron WF. 2013. The divergence, actions, roles, and relatives of sodium-coupled bicarbonate transporters. Physiological Reviews 93, 803-959.

Gao H, Wang Y, Fei X, Wright DA, Spalding MH. 2015. Expression activation and functional analysis of HLA3, a putative inorganic carbon transporter in *Chlamydomonas reinhardtii*. The Plant Journal 82, 1-11.

Nessim RB, Tadros HRZ, Abou Taleb AEA, Moawad MN. 2015. Chemistry of the Egyptian Mediterranean coastal waters. Egyptian Journal of Aquatic Research 41, 1-10.

Zhang Q, Jian L, Yao D, Rao B, Xia Y, Hu K, Li S, Shen Y, Cao M, Qin A, Zhao J, Cao Y. 2023. The structural basis of the pH-homeostasis mediated by the Cl^-/HCO_3^- exchanger, AE2. Nature Communications 14, 1812.

Reithmeier RAF. 2001. A membrane metabolon linking carbonic anhydrase with chloride/bicarbonate anion exchangers. Blood Cells Molecules & Diseases 27, 85-89.

Reithmeier RAF, Casey JR, Kalli AC, Sansom MSP, Alguel Y, Iwata S. 2016. Band 3, the human red cell chloride/bicarbonate anion exchanger (AE1, SLC4A1), in a structural context. Biochimica Et Biophysica Acta-Biomembranes 1858, 1507-1532.

Jennings ML. 2021. Cell physiology and molecular mechanism of anion transport by erythrocyte band 3/AE1. American Journal of Physiology Cell Physiology 321, C1028-C1059.

Schultz SG, Wilson NL, Epstein W. 1962. Cation transport in *Escherichia coli*. II. Intracellular chloride concentration. Journal of General Physiology 46, 159-166.

Garcia-Celma J, Szydelko A, Dutzler R. 2013. Functional characterization of a ClC transporter by solid-supported membrane electrophysiology. Journal of General Physiology 141, 479-491.

Ritchie RJ. 1992. The cyanobacterium *Synechococcus* R-2 (*Anacystis nidulans, S. leopoliensis*) PCC 7942 has a sodium-dependent chloride transporter. Plant, Cell & Environment 15, 163-177.

Hagemann M. 2011. Molecular biology of cyanobacterial salt acclimation. Fems Microbiology Reviews 35, 87-123.

Davis-Kaplan SR, Askwith CC, Bengtzen AC, Radisky D, Kaplan J. 1998. Chloride is an allosteric effector of copper assembly for the yeast multicopper oxidase Fet3p: An unexpected role for intracellular chloride channels. Proceedings of the National Academy of Sciences 95, 13641-13645.

Tulloch LB, Morgan HP, Hannaert V, Michels PAM, Fothergill-Gilmore LA, Walkinshaw MD. 2008. Sulphate removal induces a major conformational change in *Leishmania mexicana* pyruvate kinase in the crystalline state. Journal of Molecular Biology 383, 615-626.

Perutz MF, Shih DTb, Williamson D. 1994. The Chloride effect in human haemoglobin: A new kind of allosteric mechanism. Journal of Molecular Biology 239, 555-560.

Xu M, Bernat G, Singh A, Mi HL, Rogner M, Pakrasi HB, Ogawa T. 2008. Properties of mutants of *Synechocystis* sp strain PCC6803 lacking inorganic carbon sequestration systems. Plant and cell physiology 49, 1672-1677.

Van Mooy BA, Rocap G, Fredricks HF, Evans CT, Devol AH. 2006. Sulfolipids dramatically decrease phosphorus demand by picocyanobacteria in oligotrophic marine environments. Proceedings of the National Academy of Sciences of the United States of America 103, 8607-8612.

Selim KA, Haffner M, Mantovani O, Albrecht R, Zhu H, Hagemann M, Forchhammer K, Hartmann MD. 2023. Carbon signaling protein SbtB possesses atypical redox-regulated apyrase activity to facilitate regulation of bicarbonate transporter SbtA. Proceedings of the National Academy of Sciences of the United States of America 120, e2205882120.

Liu XY, Hou WT, Wang L, Li B, Chen Y, Chen Y, Jiang YL, Zhou CZ. 2021. Structures of cyanobacterial bicarbonate transporter SbtA and its complex with PII-like SbtB. Cell Discovery 7, 63.

Ray DK, Mueller ND, West PC, Foley JA. 2013. Yield trends are insufficient to double global crop production by 2050. PloS one 8, e66428.

Colmenero-Flores JM, Franco-Navarro JD, Cubero-Font P, Peinado-Torrubia P, Rosales MA. 2019. Chloride as a beneficial macronutrient in higher plants: New roles and regulation. International Journal of Molecular Sciences 20, 4686.

Demmig B, Gimmler H. 1983. Properties of the isolated intact chloroplast at cytoplasmic K concentrations : I. Light-induced cation uptake into intact chloroplasts is driven by an electrical potential difference. Plant physiology 73, 169-174.

Robinson SP, Downton WJ. 1984. Potassium, sodium, and chloride content of isolated intact chloroplasts in relation to ionic compartmentation in leaves. Archives of Biochemistry and Biophysics 228, 197-206.

Franco-Navarro JD, Rosales MA, Cubero-Font P, Calvo P, Alvarez R, Diaz-Espejo A, Colmenero-Flores JM. 2019. Chloride as a macronutrient increases water-use efficiency by anatomically driven reduced stomatal conductance and increased mesophyll diffusion to CO_2. Plant Journal, 1-17.

Demmig B, Winter K. 1986. Sodium, potassium, chloride and proline concentrations of chloroplasts isolated from a halophyte, *Mesembryanthemum crystallinum* L. Planta 168, 421-426.

Rourke LM, Au EK, Byrt CS, Long BM, Price GD. 2025. Dataset for "Functional characterisation of bicarbonate transporters from the cyanobacterial SbtA2 family and subsequent expression in tobacco". Mendeley Data. doi:10.17632/wrwjkyn6bn.1

Letunic I, Bork P. 2024. Interactive Tree of Life (iTOL) v6: recent updates to the phylogenetic tree display and annotation tool. Nucleic Acids Research 52, W78-W82.

Biebl H, Pukall R, Lünsdorf H, Schulz S, Allgaier M, Tindall BJ, Wagner-Döbler I. 2007. Description of *Labrenzia alexandrii* gen. nov., sp. nov., a novel alphaproteobacterium containing bacteriochlorophyll a, and a proposal for reclassification of *Stappia aggregata* as *Labrenzia aggregata* comb. nov., of *Stappia marina* as *Labrenzia marina* comb. nov. and of *Stappia alba* as *Labrenzia alba* comb. nov., and emended descriptions of the genera *Pannonibacter*, *Stappia* and *Roseibium*, and of the species *Roseibium denhamense* and *Roseibium*

hamelinense. International Journal of Systematic and Evolutionary Microbiology 57, 1095-1107.

Tables

Table 1: The affinity for HCO_3^- of SbtA2 homologues

	WH5701	WH5701 Cl^- [a]	RCC307	CB0205
V_{max}	1.34 ± 0.07	2.19	0.38 ± 0.06	0.34 ± 0.02
K_m (μM)	146 ± 33	140	147 ± 16	197 ± 21

The K_m (μM) and V_{max} (μmol Ci·OD_{600}^{-1}·h^{-1}) of the transporters in the presence of 20 mM NaCl in the assay buffer, mean from 3 assays. [a] Results for WH5701 Cl^- are from a single HCO_3^- uptake experiment assessing the K_m in of SbtA2-WH5701 in the presence of 100 mM NaCl in the assay buffer.

Table 2: The estimated Ci pool sizes of *E. coli* cells expressing SbtA2 homologues

	WH5701 [c]	WH5701 [d]	SbtA1-7942 [c]	EV [c]	EV [d]
Ci pool (mM) [a]	5.5 - 8	15 - 24	2 - 3	0.2	0.3
Fold increase [b]	30 - 36	57 - 69	12-14	-	-

[a] Ci pool sizes are estimated based on cell volumes from our previous study (Du et al., 2014) and from uptake rates over a 30 sec period during silicone-oil centrifugation assays using 0.5 mM $NaH^{14}CO_3$. [b] Fold increase in pool size is compared with estimated pool sizes in empty vector (EV) controls in 30 sec uptake assays. [c] assessed in the presence of 20 mM NaCl. [d] assessed in the presence of 200 mM Cl^-.

Figure Legends

Figure 1: Phylogenetic tree showing the relative protein relationships between members of the SbtA family across cyanobacteria.
The primary sequence alignment, and derived tree, were prepared using Geneious Prime software and iTol (Letunic and Bork, 2024). The SbtA2 family is highlighted in blue and the SbtA1 family in pink. The internal size marker indicates 0.1 substitutions per residue. Red branches indicate α-cyanobacteria and purple branches indicate β-cyanobacteria. Coloured bold text indicates that HCO_3^- uptake activity has been assessed with those and in black bold text demonstrating no function in E. coli (this study and Du *et al.*, 2014). The outgroup SbtA1 from *Labrenzia* DFL-11, an α-proteobacterium found in close association with dinoflagellates of the *Alexandrium* genus (Biebl *et al.*, 2007), was previously assessed for function by (Du *et al.*, 2014).

Figure 2: **The HCO_3^- transport function of SbtA2 was assessed using complementation assays and HCO_3^- uptake assays.**
(A) Cultures of CAfree E. coli expressing SbtA2 homologues were adjusted to the same density prior to being spotted onto LB-agar containing 100 μM IPTG and grown at ambient (0.04%) or 4% CO_2 for ~20 h. The growth of SbtA2 members (Synechococcus WH5701, RCC307, CB0205 and Prochlorococcus MIT0701 and MIT9313) were compared to a negative control (empty vector; EV) and a positive control (SbtA1 from Synechococcus elongatus PCC7942; SbtA1-7942). **(B)** The HCO_3^- uptake activity of SbtA2-WH5701 (A2), SbtA1 from Synechococcus PCC7942 (SbtA1-7942; A1) and empty vector (EV). n=12 from 3 biological replicates. **(C)** HCO_3^- uptake activity of SbtA2 from Synechococcus WH5701 (WH), RCC307 (RCC) and CB0205 (CB). n=12 from 3 biological replicates. HCO_3^- uptake assay buffer composition: BTP - H_2SO_4 pH 7.5 + 20 mM NaCl. Different letters indicate significantly different means when analysed by one-way ANOVA ($P<0.05$).

Figure 3: Assessment of the counter-ion driving the HCO_3^- uptake function of SbtA2.
Analysis of ion dependency was determined using HCO_3^- uptake assays in DH5α strain of E. coli. Values presented have empty vector rates for each condition subtracted. Different letters indicate significantly different means when analysed by one-way ANOVA ($P<0.05$). **(A)** The HCO_3^- uptake activity of SbtA2-WH5701 (SbtA2) and SbtA1-7942 (SbtA1) was assessed in the presence of 0, 1, 5 or 20 mM NaCl. Assay buffer composition: 20 mM BTP-H_2SO_4 pH 7.5 + (0, 1, 5, or 20 mM NaCl). Na^+ provided by $NaH^{14}CO_3/KHCO_3$ was ~20 μM. The connecting line represents the mean; n= 3-4 from 1 biological replicate. **(B)** The HCO_3^- uptake rates of SbtA2-WH5701 in the presence of 0 and 20 mM NaCl in the assay buffer were compared. Assay buffer composition: 20 mM BTP-H_2SO_4 pH 7.5 + (0 or 20 mM NaCl). Data presented as mean ± SD; n=27 from 8 biological replicates. **(C)** The HCO_3^- uptake activity of SbtA2-WH5701 was measured in response to an increase in NaCl concentration in the assay buffer. Uptake assay buffer composition: 20 mM BTP-H_2SO_4 pH 7.5 + 10 mM K_2HPO_4 + (0, 50,

100 or 200 mM NaCl). n=11-16 from 3-4 biological replicates. **(D)** The HCO_3^- uptake activity of SbtA2-WH5701 was assessed in the presence of various salts; no additional NaCl, 100 mM NaCl, 100 mM KCl, 100 mM LiCl and 100 mM $NaNO_3$ added to the assay buffer of 20 mM BTP-H_2SO_4 pH 7.5. Salt concentrations added to the uptake buffer are in mM. 20 µM Na^+ was supplied by $NaH^{14}CO_3$. Data presented as mean ± SD; n=16-20 from 4-5 biological replicates. **(E)** The HCO_3^- uptake activity of SbtA2-WH5701 was assessed in response to different salts; no additional NaCl, 100 mM NaCl, 50 mM $MgCl_2$, 50 mM $MgSO_4$ and 50 mM $NaSO_4$, 200 mM NaCl or 100 mM $MgCl_2$ added to the assay buffer of 20 mM BTP-H_2SO_4 pH 7.5. 20 µM Na^+ was supplied by $NaH^{14}CO_3$. Data presented as mean ± SD; n=8-12 from 2-3 biological replicates.

Figure 4: The affinity (K_m) for HCO_3^- was determined for SbtA2 from *Synechococcus* WH5701.
The affinity for HCO_3^- was estimated using Ci uptake assays performed in response to increasing exogenous HCO_3^- concentrations in E. coli DH5α. The HCO_3^- affinity of SbtA2-WH5701 was assessed in the presence of 20 mM NaCl or 100 mM NaCl. Assay buffer composition: BTP - H_2SO_4 pH 7.5 + (20 mM NaCl or 100 mM NaCl). HCO_3^- uptake rates at each HCO_3^- concentration had empty vector rates specific for that condition subtracted. Similar trends were observed across experiments although the activity values varied, as a result representative data from single experiments are shown. Individual data values are shown along with their fitted Michaelis-Menten curve which is presented as a solid line. Curve fitting protocols are stated in the materials and methods section.

Figure 5: Assessment of the effect of SbtB2 on SbtA2 HCO_3^- transport function.
(A) Cultures of CAfree were adjusted to the same density prior to spotting onto LB-agar containing antibiotics and 100 µM IPTG and grown at ambient (0.04%) or 4% CO_2 for ~20 h. The cultures assessed included positive control SbtA1 from *Synechococcus* PCC7942, (SbtA1-7942) SbtA2:B2-HA from *Synechococcus* WH5701, RCC307, and CB0205, a negative control (empty vector; EV) and positive controls (SbtA2-WH5701, SbtA2-RCC307, SbtA2-CB0205). **(B)** The relative HCO_3^- uptake activity of DH5α *E. coli* carrying SbtA2:B2-HA-WH5701 and SbtA2:B2-WH5701 compared to SbtA2-WH5701 (A2). Assay buffer composition: 20 mM BTP-H_2SO_4 pH 7.5. Data presented as the mean with empty vector control subtracted ± SD; n=8 from 2 biological replicates. **(C)** The relative HCO_3^- uptake activity of DH5α *E. coli* carrying *lacI*^{q}-SbtA2-H6:B2-HA-WH5701 (*l*AB2), *lacI*^{q}-SbtA2-H6:*tet*-B2-HA-WH5701 (*l*A2*t*B2) and *lacI*^{q}-SbtB2-HA:A2-H6-WH5701 (*l*BA2) compared to *lacI*^{q}-SbtA2-H6-WH5701 (*l*A2). Assay buffer composition: 20 mM BTP-H_2SO_4 pH 7.5 + 200 mM NaCl. Data presented as the mean ± SD with empty vector controls subtracted; n= 12 from 3 biological replicates.

Figure 6 : Phenotypic measurements of *N. tabacum* expressing SbtA-HAH6-WH5701 (Tob^{SbtA}) compared to wild-type (Tob^{WT}) plants.
(A) The heights of plants were measured 63 days post cotyledon emergence (pce) from the base of the plants to the base of the apical meristem. The data is presented as means ± SD; n=6. **(B)** Each

plant was harvested at the base of the stem 63 days pce and the fresh weight was measured. **(C)** The harvested plants were dried for 7 days at 80°C and the weight were measured. Data presented as mean ± SD; n=6. **(D-F)** A/C_{int} curves were measured on plants 30 ± 5 cm in height on young fully expanded leaves of similar size using a Licor 6800 with the following parameters; photon flux density 1500 $\mu mol \cdot m^{-2} \cdot s^{-1}$, at 25°C and photosynthetic measurements taken at 400, 200, 100, 50,150, 250, 400, 600, 800, 1200, 400 $\mu mol \cdot mol^{-1}$ CO_2. Data presented as mean ± SD. n= 3-5 for Tob^{SbtA2} and n=9 for Tob^{WT}. **(G)** $\Delta^{13}C$ was determined from dry matter samples taken when the plants were 30 ± 5 cm in height. Asterisk (*) indicates significant difference between Tob^{SbtA} and Tob^{WT} plants as determined using unpaired *t*-test (P>0.05). Data presented as mean ± SD; n=4-6. **(H)** Comparison of $Tob^{SbtA\text{-}ubi}$ and Tob^{WT} plants 63 days post cotyledon emergence.

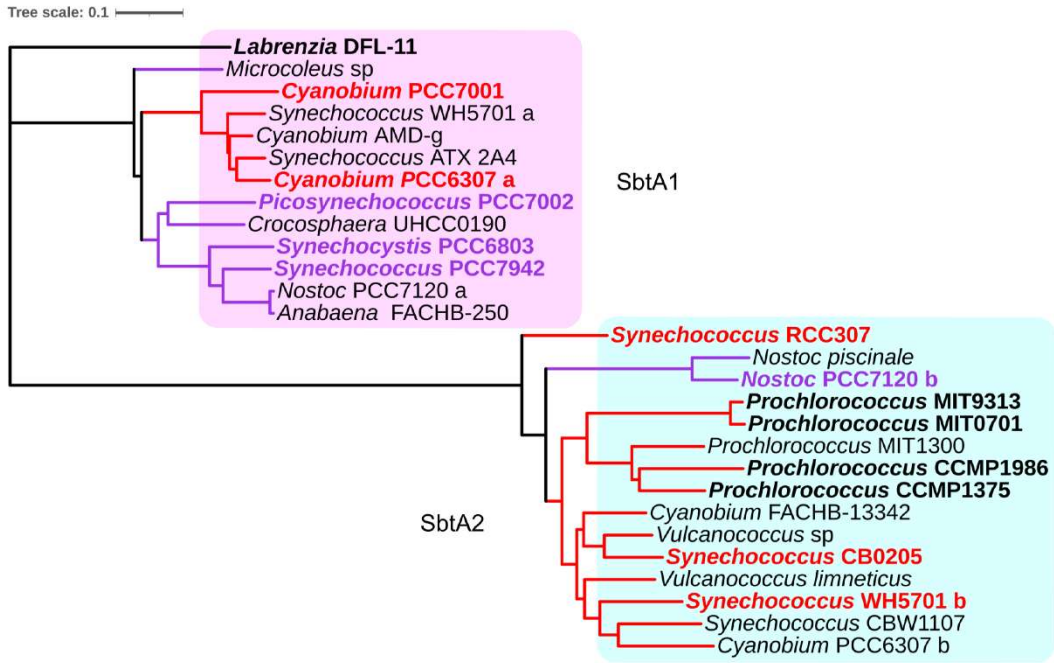

Figure 1: Phylogenetic tree showing the relative protein relationships between members of the SbtA family across cyanobacteria.

The primary sequence alignment, and derived tree, were prepared using Geneious Prime software and iTol (Letunic and Bork, 2024). The SbtA2 family is highlighted in blue and the SbtA1 family in pink. The internal size marker indicates 0.1 substitutions per residue. Red branches indicate α-cyanobacteria and purple branches indicate β-cyanobacteria. Coloured bold text indicates that HCO_3^- uptake activity has been assessed with those and in black bold text demonstrating no function in E. coli (this study and Du *et al.*, 2014). The outgroup SbtA1 from *Labrenzia* DFL-11, an α-proteobacterium found in close association with dinoflagellates of the *Alexandrium* genus (Biebl *et al.*, 2007), was previously assessed for function by (Du *et al.*, 2014).

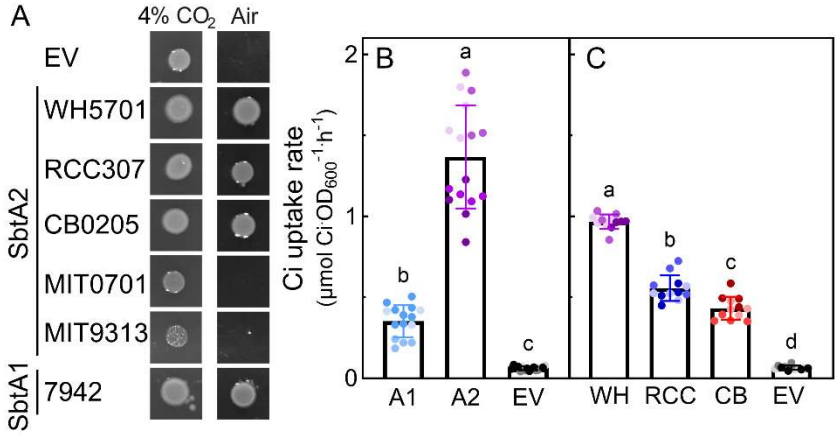

Figure 2: **The HCO_3^- transport function of SbtA2 was assessed using complementation assays and HCO_3^- uptake assays.**

(A) Cultures of CAfree E. coli expressing SbtA2 homologues were adjusted to the same density prior to being spotted onto LB-agar containing 100 µM IPTG and grown at ambient (0.04%) or 4% CO_2 for ~20 h. The growth of SbtA2 members (Synechococcus WH5701, RCC307, CB0205 and Prochlorococcus MIT0701 and MIT9313) were compared to a negative control (empty vector; EV) and a positive control (SbtA1 from Synechococcus elongatus PCC7942; SbtA1-7942). **(B)** The HCO_3^- uptake activity of SbtA2-WH5701 (A2), SbtA1 from Synechococcus PCC7942 (SbtA1-7942; A1) and empty vector (EV). n=12 from 3 biological replicates. **(C)** HCO_3^- uptake activity of SbtA2 from Synechococcus WH5701 (WH), RCC307 (RCC) and CB0205 (CB). n=12 from 3 biological replicates. HCO_3^- uptake assay buffer composition: BTP - H_2SO_4 pH 7.5 + 20 mM NaCl. Different letters indicate significantly different means when analysed by one-way ANOVA ($P<0.05$).

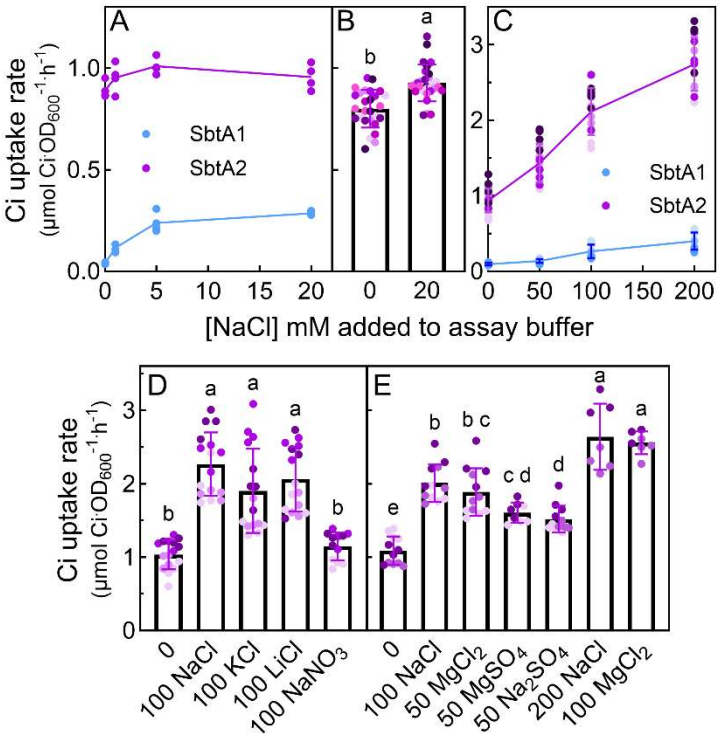

Figure 3: Assessment of the counter-ion driving the HCO_3^- uptake function of SbtA2. Analysis of ion dependency was determined using HCO_3^- uptake assays in DH5α strain of E. coli. Values presented have empty vector rates for each condition subtracted. Different letters indicate significantly different means when analysed by one-way ANOVA (P<0.05). **(A)** The HCO_3^- uptake activity of SbtA2-WH5701 (SbtA2) and SbtA1-7942 (SbtA1) was assessed in the presence of 0, 1, 5 or 20 mM NaCl. Assay buffer composition: 20 mM BTP-H_2SO_4 pH 7.5 + (0, 1, 5, or 20 mM NaCl). Na^+ provided by $NaH^{14}CO_3/KHCO_3$ was ~20 µM. The connecting line represents the mean; n= 3-4 from 1 biological replicate. **(B)** The HCO_3^- uptake rates of SbtA2-WH5701 in the presence of 0 and 20 mM NaCl in the assay buffer were compared. Assay buffer composition: 20 mM BTP-H_2SO_4 pH 7.5 + (0 or 20 mM NaCl). Data presented as mean ± SD; n=27 from 8 biological replicates. **(C)** The HCO_3^- uptake activity of SbtA2-WH5701 was measured in response to an increase in NaCl concentration in the assay buffer. Uptake assay buffer composition: 20 mM BTP-H_2SO_4 pH 7.5 + 10 mM K_2HPO_4 + (0, 50, 100 or 200 mM NaCl). n=11-16 from 3-4 biological replicates. **(D)** The HCO_3^- uptake activity of SbtA2-WH5701 was assessed in the presence of various salts; no additional NaCl, 100 mM NaCl, 100 mM KCl, 100 mM LiCl and 100 mM $NaNO_3$ added to the assay buffer of 20 mM BTP-H_2SO_4 pH 7.5. Salt concentrations added to the uptake buffer are in mM. 20 µM Na^+ was supplied by $NaH^{14}CO_3$. Data presented as mean ± SD; n=16-20 from 4-5 biological replicates. **(E)** The HCO_3^- uptake activity of SbtA2-WH5701 was assessed in response to different salts; no additional NaCl, 100 mM NaCl, 50 mM $MgCl_2$, 50 mM $MgSO_4$ and 50 mM $NaSO_4$, 200 mM NaCl or 100 mM $MgCl_2$ added to the assay buffer of 20 mM BTP-H_2SO_4 pH 7.5. 20 µM Na^+ was supplied by $NaH^{14}CO_3$. Data presented as mean ± SD; n=8-12 from 2-3 biological replicates.

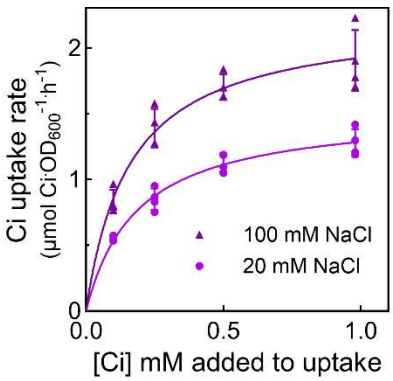

Figure 4: The affinity (K_m) for HCO_3^- was determined for SbtA2 from *Synechococcus* WH5701. The affinity for HCO_3^- was estimated using Ci uptake assays performed in response to increasing exogenous HCO_3^- concentrations in E. coli DH5α. The HCO_3^- affinity of SbtA2-WH5701 was assessed in the presence of 20 mM NaCl or 100 mM NaCl. Assay buffer composition: BTP - H_2SO_4 pH 7.5 + (20 mM NaCl or 100 mM NaCl). HCO_3^- uptake rates at each HCO_3^- concentration had empty vector rates specific for that condition subtracted. Similar trends were observed across experiments although the activity values varied, as a result representative data from single experiments are shown. Individual data values are shown along with their fitted Michaelis-Menten curve which is presented as a solid line. Curve fitting protocols are stated in the materials and methods section.

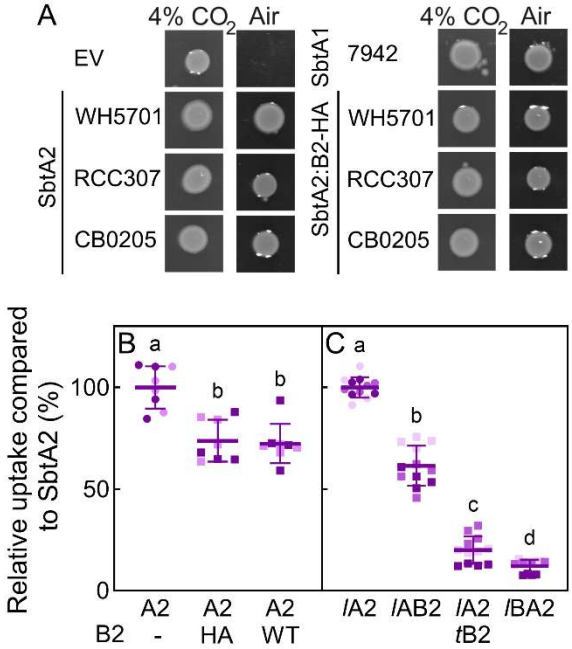

Figure 5: Assessment of the effect of SbtB2 on SbtA2 HCO_3^- transport function.
(A) Cultures of CAfree were adjusted to the same density prior to spotting onto LB-agar containing antibiotics and 100 µM IPTG and grown at ambient (0.04%) or 4% CO_2 for ~20 h. The cultures assessed included positive control SbtA1 from *Synechococcus* PCC7942, (SbtA1-7942) SbtA2:B2-HA from *Synechococcus* WH5701, RCC307, and CB0205, a negative control (empty vector; EV) and positive controls (SbtA2-WH5701, SbtA2-RCC307, SbtA2-CB0205). **(B)** The relative HCO_3^- uptake activity of DH5α *E. coli* carrying SbtA2:B2-HA-WH5701 and SbtA2:B2-WH5701 compared to SbtA2-WH5701 (A2). Assay buffer composition: 20 mM BTP-H_2SO_4 pH 7.5. Data presented as the mean with empty vector control subtracted ± SD; n=8 from 2 biological replicates. **(C)** The relative HCO_3^- uptake activity of DH5α *E. coli* carrying *lacI*^{q}-SbtA2-H6:B2-HA-WH5701 (*l*AB2), *lacI*^{q}-SbtA2-H6:*tet*-B2-HA-WH5701 (*l*A2*t*B2) and *lacI*^{q}-SbtB2-HA:A2-H6-WH5701 (*l*BA2) compared to *lacI*^{q}-SbtA2-H6-WH5701 (*l*A2). Assay buffer composition: 20 mM BTP-H_2SO_4 pH 7.5 + 200 mM NaCl. Data presented as the mean ± SD with empty vector controls subtracted; n= 12 from 3 biological replicates.

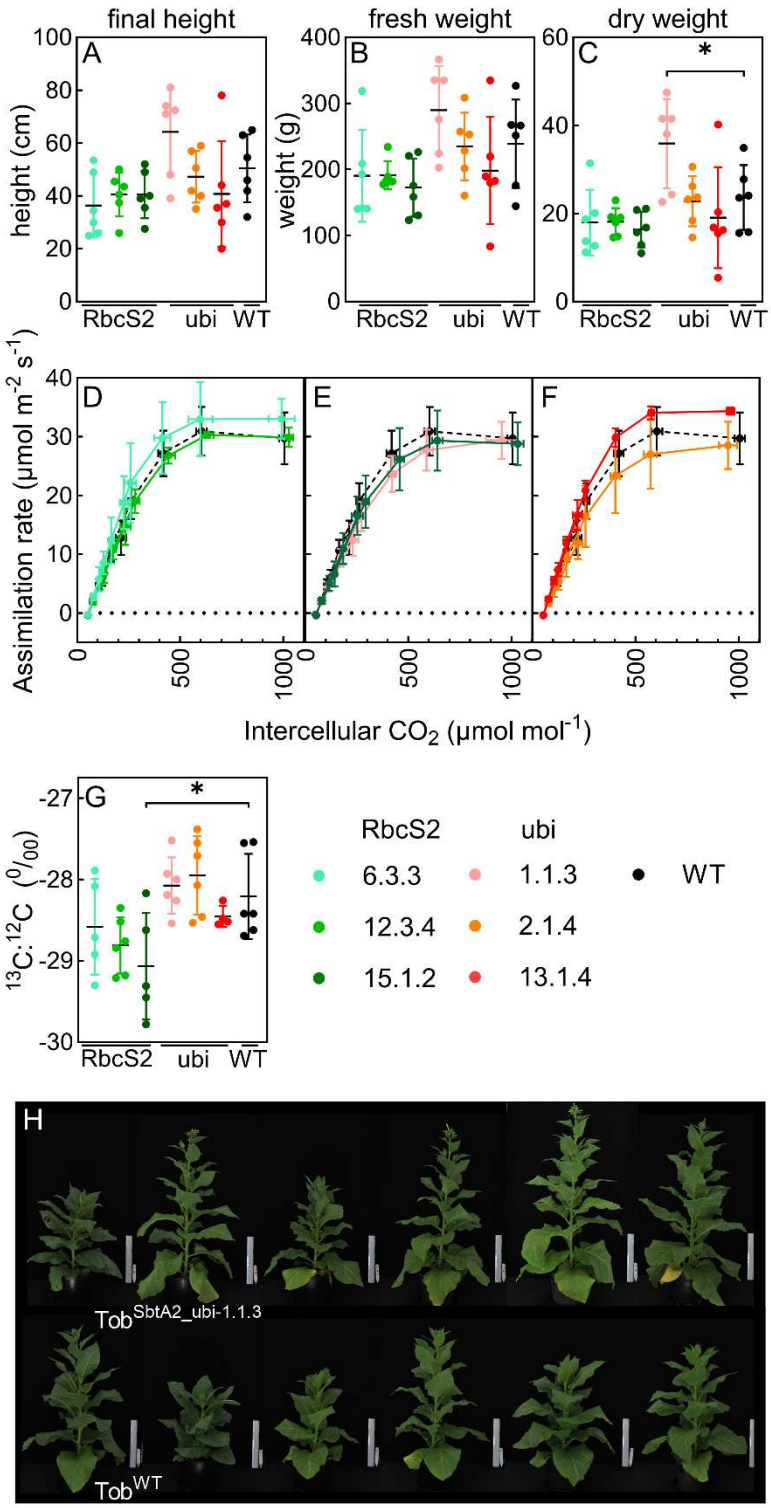

Figure 6 : Phenotypic measurements of *N. tabacum* expressing SbtA-HAH6-WH5701 (Tob^{SbtA}) compared to wild-type (Tob^{WT}) plants.

(A) The heights of plants were measured 63 days post cotyledon emergence (pce) from the base of the plants to the base of the apical meristem. The data is presented as means ± SD; n=6. **(B)** Each plant was harvested at the base of the stem 63 days pce and the fresh weight was measured. **(C)** The

harvested plants were dried for 7 days at 80°C and the weight were measured. Data presented as mean ± SD; n=6. **(D-F)** A/C_{int} curves were measured on plants 30 ± 5 cm in height on young fully expanded leaves of similar size using a Licor 6800 with the following parameters; photon flux density 1500 $\mu mol \cdot m^{-2} \cdot s^{-1}$, at 25°C and photosynthetic measurements taken at 400, 200, 100, 50,150, 250, 400, 600, 800, 1200, 400 $\mu mol \cdot mol^{-1}$ CO_2. Data presented as mean ± SD. n= 3-5 for Tob^{SbtA2} and n=9 for Tob^{WT}. **(G)** $\Delta^{13}C$ was determined from dry matter samples taken when the plants were 30 ± 5 cm in height. Asterisk (*) indicates significant difference between Tob^{SbtA} and Tob^{WT} plants as determined using unpaired *t*-test (P>0.05). Data presented as mean ± SD; n=4-6. **(H)** Comparison of $Tob^{SbtA\text{-}ubi}$ and Tob^{WT} plants 63 days post cotyledon emergence.

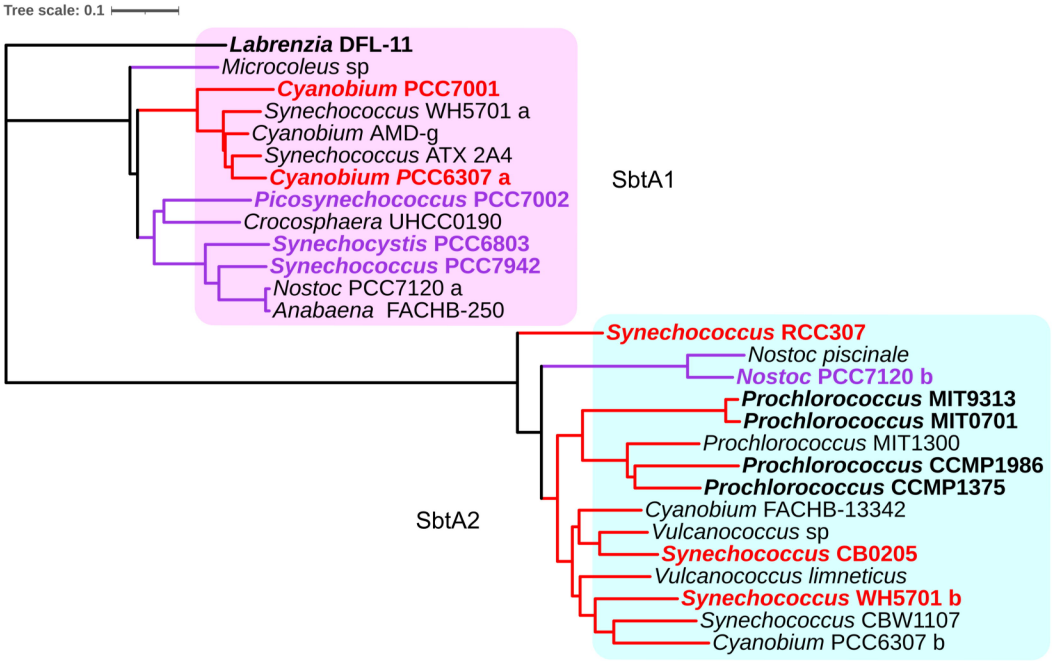
Tree scale: 0.1
Labrenzia DFL-11
Microcoleus sp
Cyanobium PCC7001
Synechococcus WH5701 a
Cyanobium AMD-g
Synechococcus ATX 2A4
Cyanobium PCC6307 a
Picosynechococcus PCC7002
Crocosphaera UHCC0190
Synechocystis PCC6803
Synechococcus PCC7942
Nostoc PCC7120 a
Anabaena FACHB-250
SbtA1
Synechococcus RCC307
Nostoc piscinale
Nostoc PCC7120 b
Prochlorococcus MIT9313
Prochlorococcus MIT0701
Prochlorococcus MIT1300
Prochlorococcus CCMP1986
Prochlorococcus CCMP1375
Cyanobium FACHB-13342
Vulcanococcus sp
Synechococcus CB0205
Vulcanococcus limneticus
Synechococcus WH5701 b
Synechococcus CBW1107
Cyanobium PCC6307 b
SbtA2

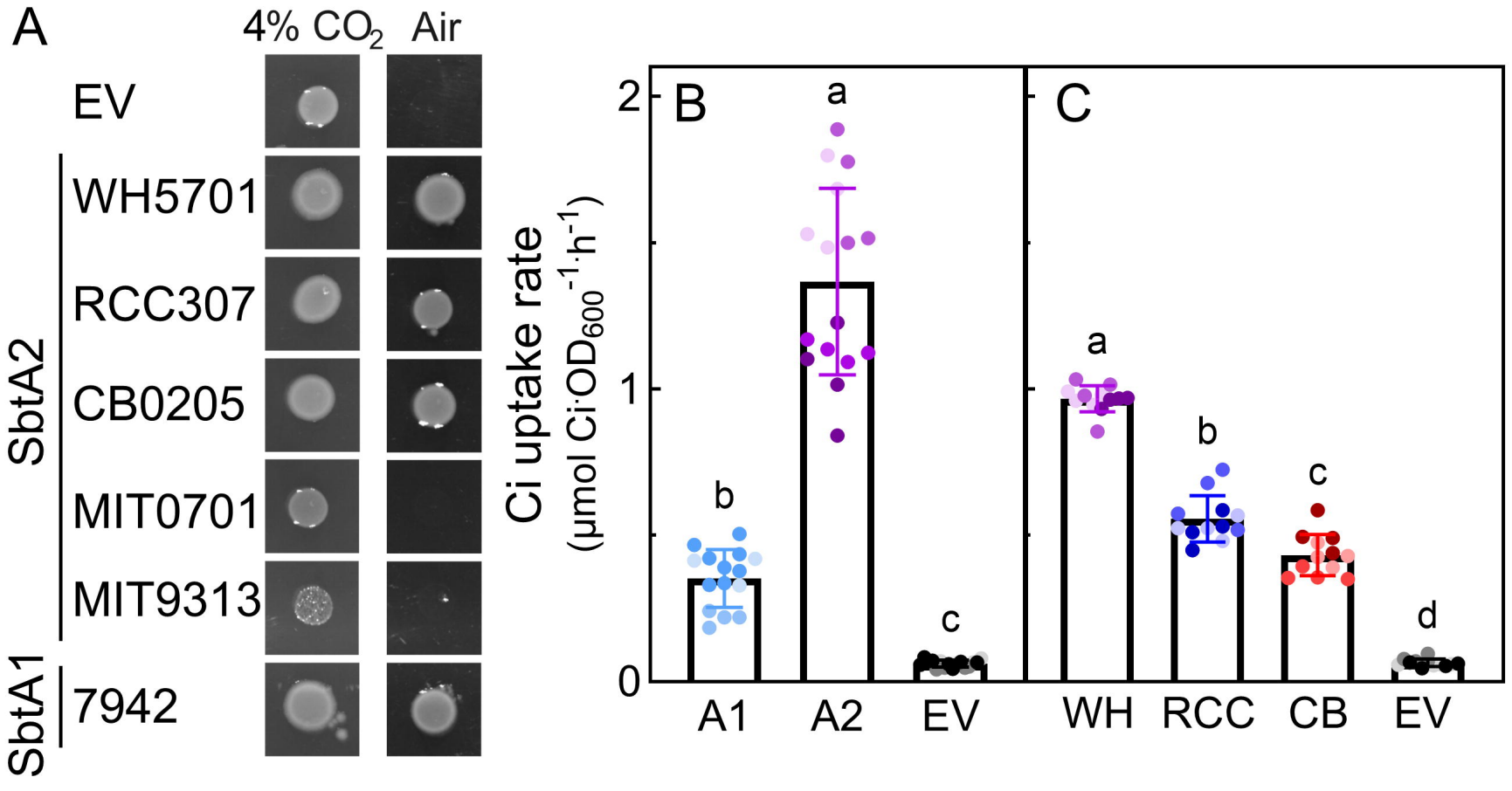
A
4% CO2
Air
EV
WH5701
RCC307
CB0205
MIT0701
MIT9313
7942
SbtA2
SbtA1
B
C
Ci uptake rate
(μmol Ci·OD600-1·h-1)
2
1
0
a
b
c
a
b
c
d
A1
A2
EV
WH
RCC
CB
EV

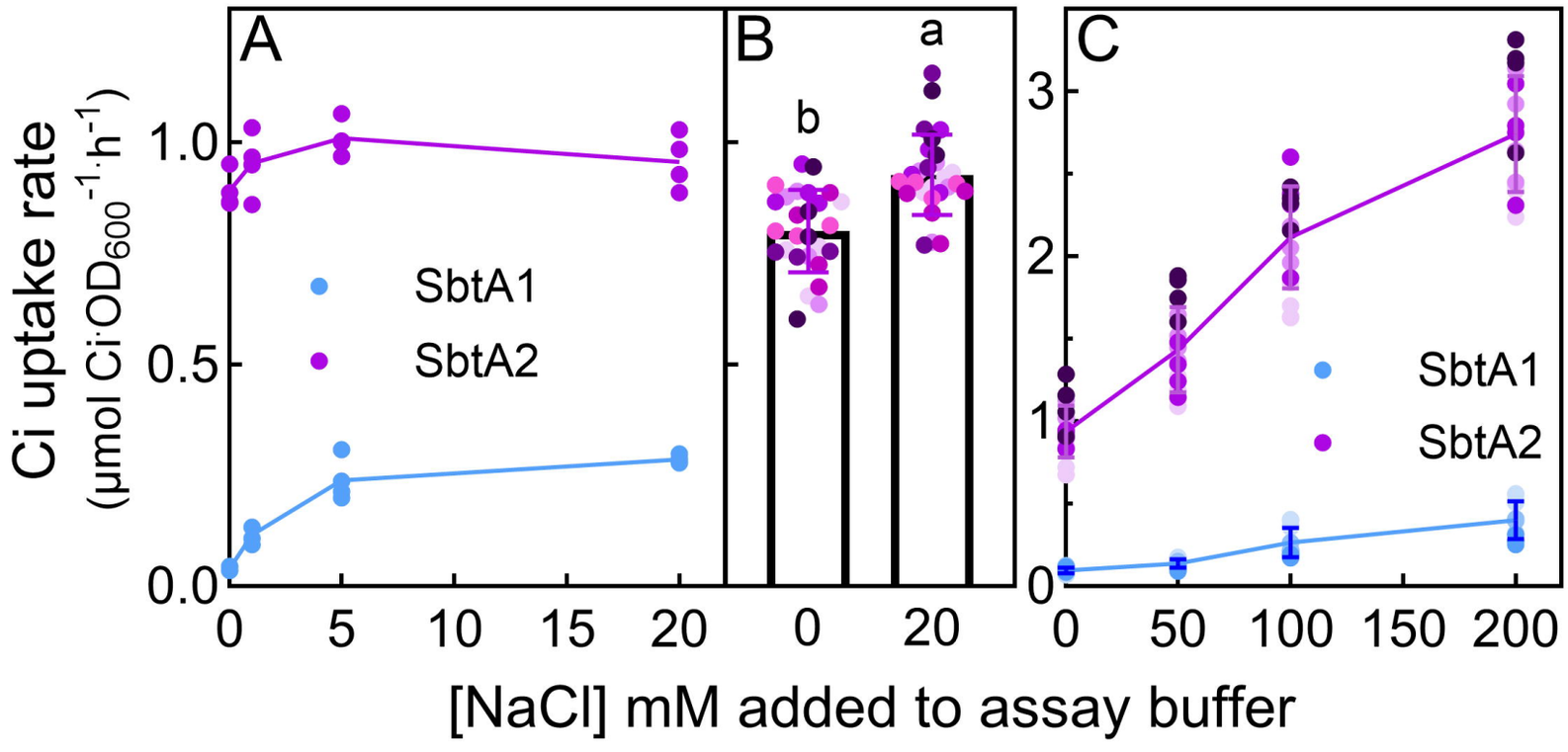
A
B
C
Ci uptake rate
(µmol Ci·OD600-1·h-1)
SbtA1
SbtA2
[NaCl] mM added to assay buffer

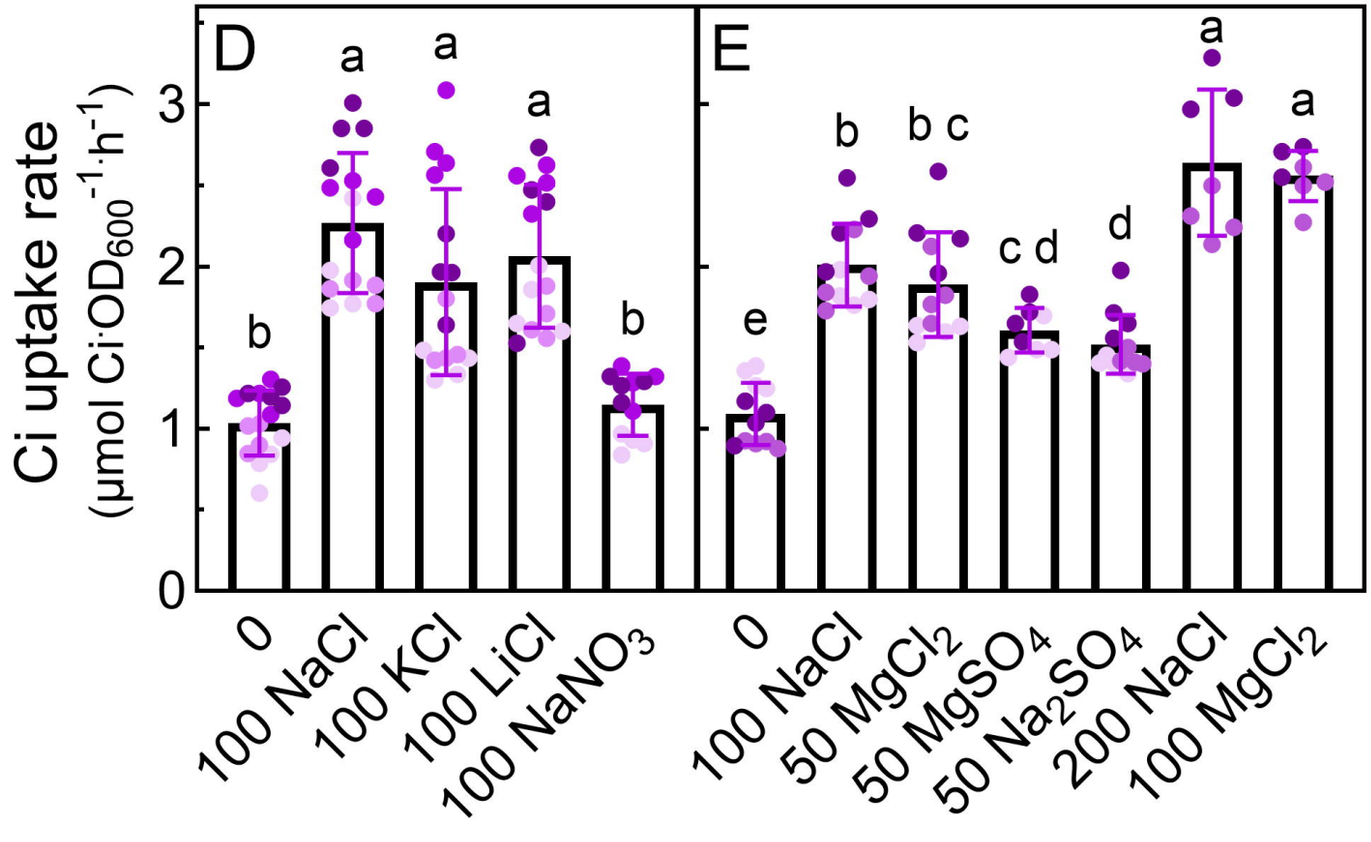
D
E
Ci uptake rate
(µmol Ci·OD600-1·h-1)
0
100 NaCl
100 KCl
100 LiCl
100 NaNO3
100 NaCl
50 MgCl2
50 MgSO4
50 Na2SO4
200 NaCl
100 MgCl2

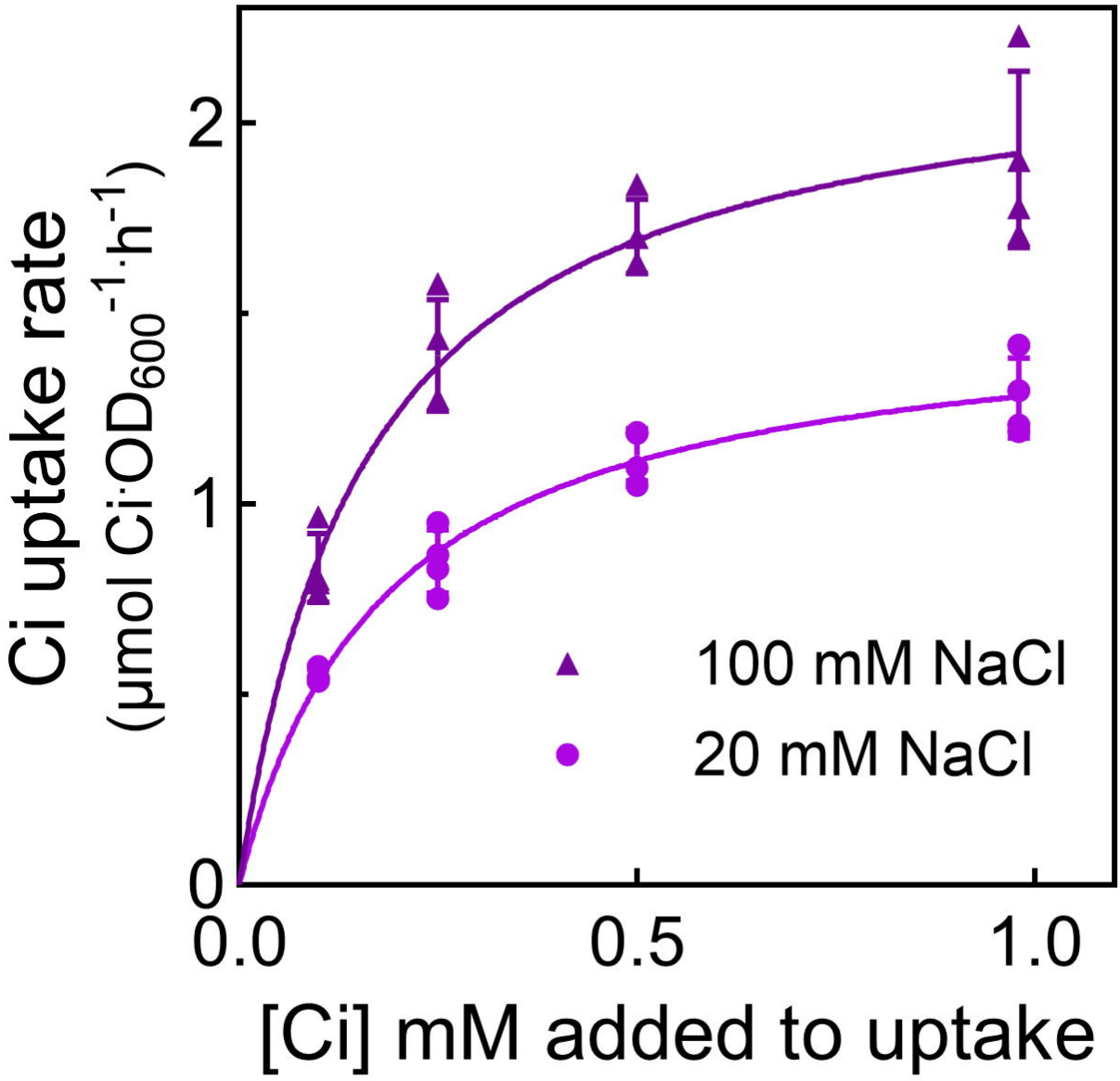
Ci uptake rate
(µmol Ci·OD600-1·h-1)
2
1
0
0.0
0.5
1.0
[Ci] mM added to uptake
100 mM NaCl
20 mM NaCl

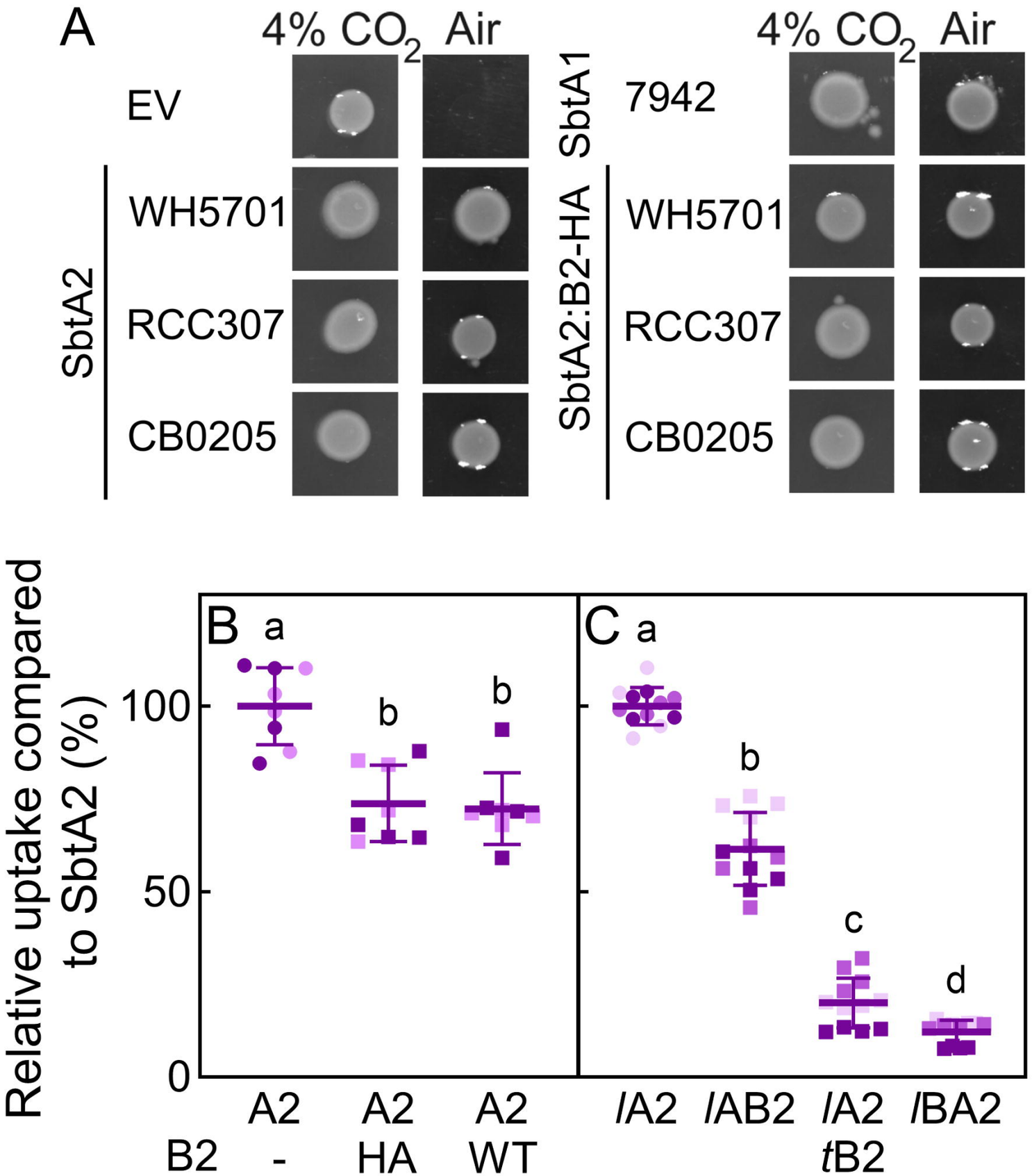
A
4% CO2
Air
EV
SbtA2
WH5701
RCC307
CB0205
SbtA1
7942
SbtA2:B2-HA
WH5701
RCC307
CB0205
Relative uptake compared to SbtA2 (%)
B
a
b
b
C
a
b
c
d
100
50
0
A2
A2
A2
/A2
/AB2
/A2
/BA2
B2
-
HA
WT
tB2

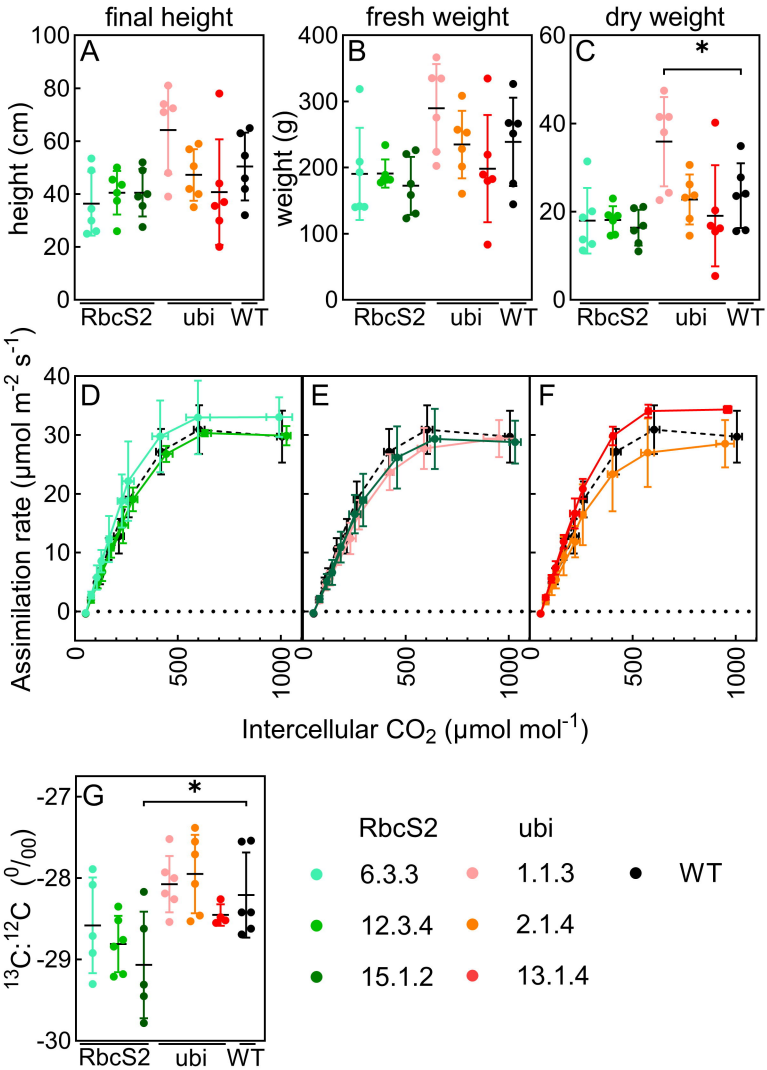
final height
fresh weight
dry weight
A
B
C
height (cm)
weight (g)
RbcS2
ubi
WT
*
D
E
F
Assimilation rate (µmol m-2 s-1)
Intercellular CO2 (µmol mol-1)
G
13C:12C (0/00)
RbcS2
6.3.3
12.3.4
15.1.2
ubi
1.1.3
2.1.4
13.1.4
WT

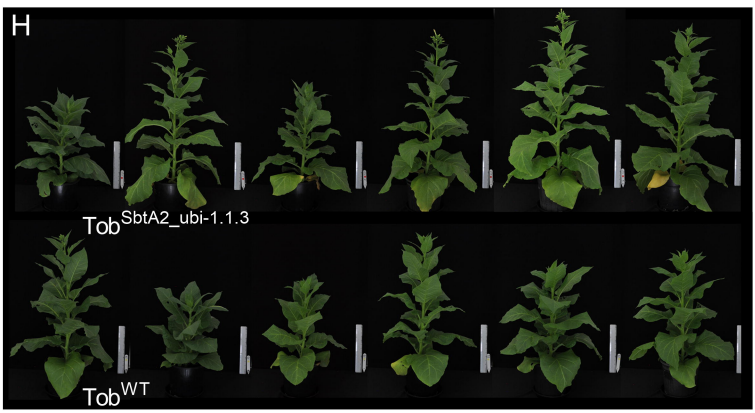
H
TobSbtA2_ubi-1.1.3
TobWT